Supporting information
for

From cyclic amines and acetonitrile to amidine zinc(II) complexes

Nina Podjed,[a] Barbara Modec,[a,]* María M. Alcaide[b] and Joaquín López-Serrano[b]

[a] Faculty of Chemistry and Chemical Technology, University of Ljubljana, Večna pot 113
1000 Ljubljana, Slovenia

[b] Instituto de Investigaciones Químicas (IIQ), Departamento de Química Inorgánica and Centro de Innovación en Química Avanzada (ORFEO-CINQA), Consejo Superior de Investigaciones Científicas (CSIC) and Universidad de Sevilla, Avenida Américo Vespucio 49, 41092 Sevilla, Spain

* Corresponding author. E-mail: barbara.modec@fkkt.uni-lj.si

1. X-ray structure determinations

Figure S1. ORTEP drawing of [Zn(quin)$_2$(pipeam)], a complex molecule of **4a**. Displacement ellipsoids are drawn at the 50% probability level. Hydrogen atoms are shown as spheres of arbitrary radii.

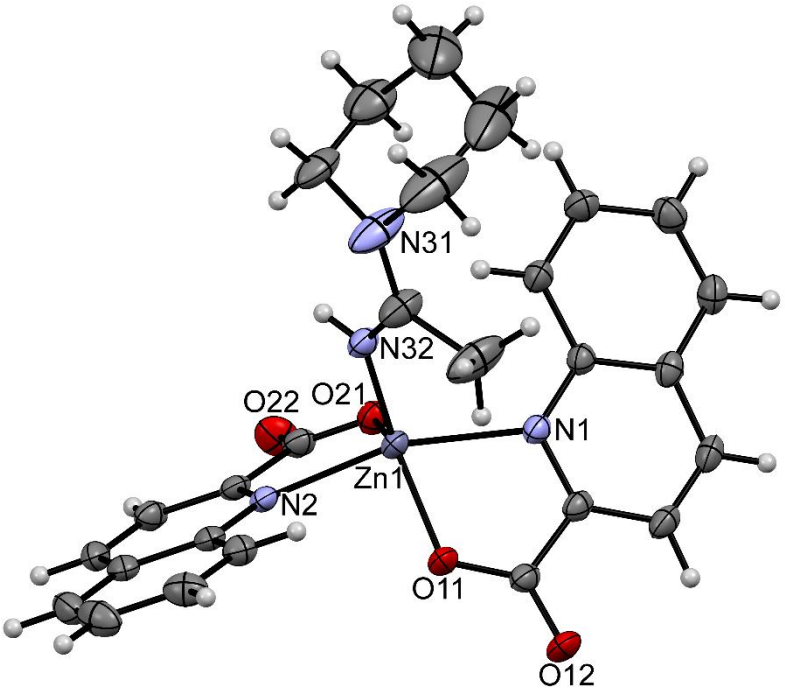

Figure S2. ORTEP drawing of *trans*-[Zn(quin)$_2$(morph)$_2$], a complex molecule of **12**. The asymmetric unit contains two halves of complex molecules. With their bonding parameters being essentially the same, only one is shown. Displacement ellipsoids are drawn at the 50% probability level. Hydrogen atoms are shown as spheres of arbitrary radii.

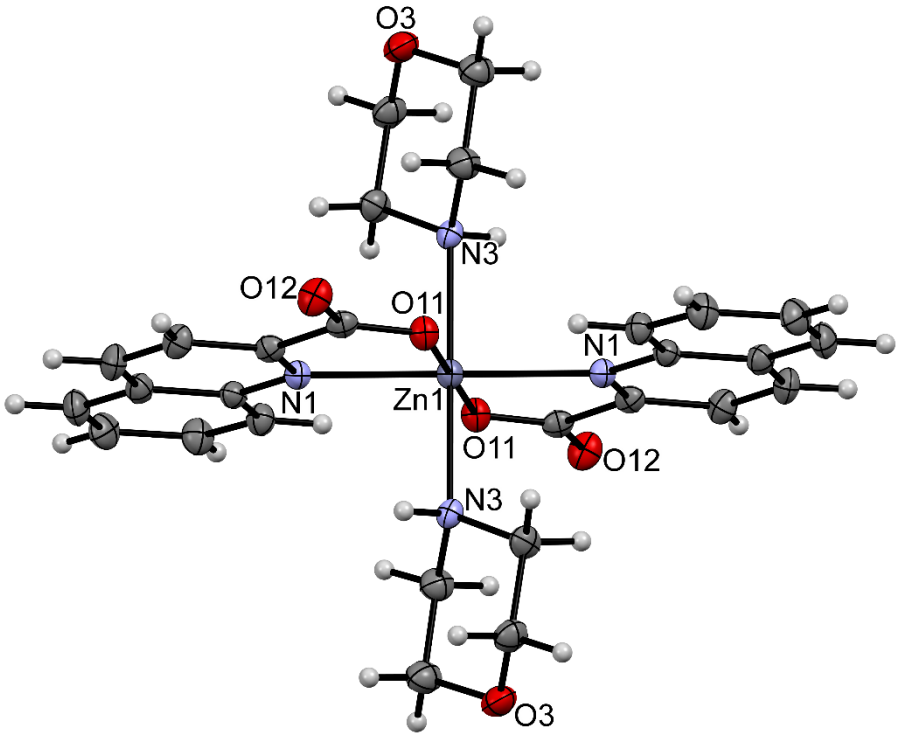

Figure S3. Overlay of $[Zn(quin)_2(pipeam)]$ molecules, done by Mercury.[S1] The RMSD value was 0.5046 and max. distance was 1.3505 Å. Color code: light grey - **4a**, pink - **4b**.

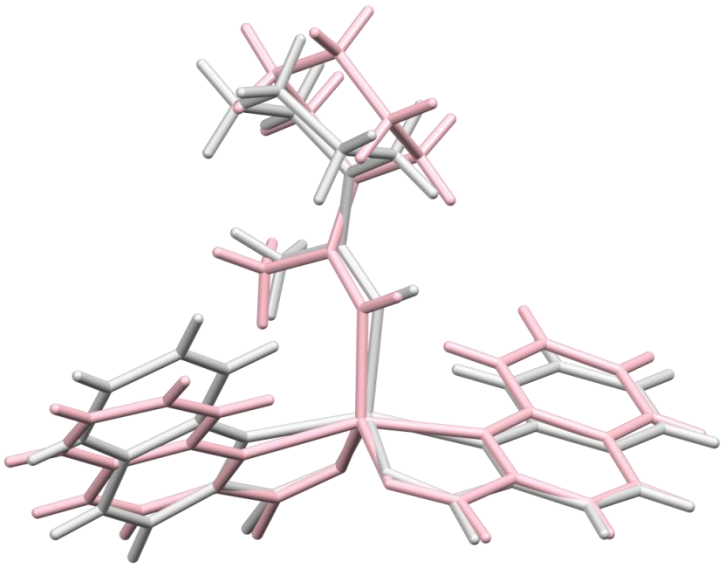

Figure S4. Overlay of the $[Zn(quin)_3]^-$ ions, as found in the polymorphic modifications of $pyroH[Zn(quin)_3]\cdot CH_3CN$, done by Mercury.[S1] The RMSD value was 0.2857 and max. distance was 0.5454 Å. Color code: pink - **8triclinic**, light grey - **8monoclinic**.

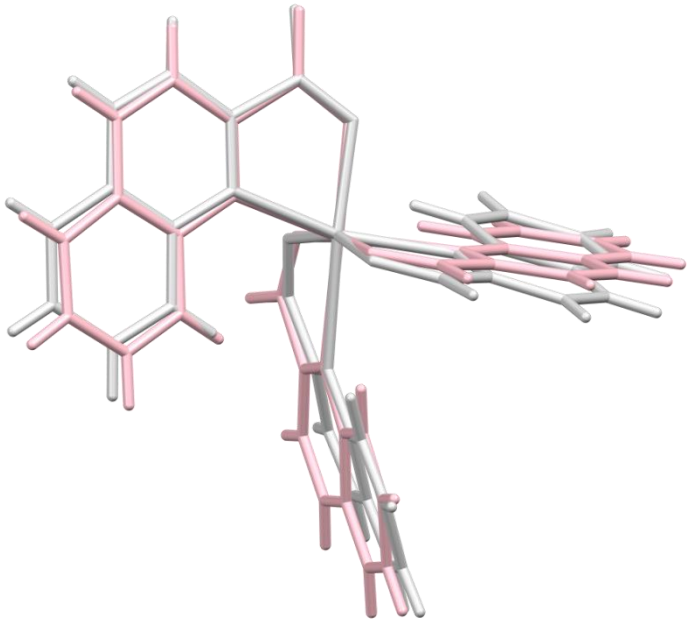

Table S1. Geometric parameters [Å, °] of amidine ligands *vs*. amidinium cations.

pipeam *vs.* pipeamH$^+$				
Compound	**4a**	**4b**	**5**	**6**
Form of amidine	pipeam	pipeam	pipeamH$^+$	pipeamH$^+$
C=N	1.289(2)	1.303(2)	1.308(2)	1.315(2)
C–N	1.352(2)	1.348(2)	1.321(2)	1.316(2)
N–C=N	124.73(17)	123.88(16)	123.31(15)	122.25(16)
C–C=N	117.56(17)	118.13(16)	116.60(15)	116.79(17)
C–C–N	117.69(17)	117.97(16)	120.07(15)	120.96(16)
pyroam *vs.* pyroamH$^+$				
Compound	**10a**	**10b**	**10c**	**11monoclinic**[a]
Form of amidine	pyroam	pyroam	pyroam	pyroamH$^+$
C=N	1.304(3)	1.295(3)	1.301(3)	1.304(5)
C–N	1.340(3)	1.334(3)	1.337(3)	1.318(5)
N–C=N	123.7(2)	123.5(2)	123.87(19)	121.7(4)
C–C=N	119.4(2)	119.6(2)	119.07(19)	119.6(4)
C–C–N	116.9(2)	116.9(2)	117.1(2)	118.7(4)

[a] Parameters for **11triclinic** are not listed owing to the low-quality X-ray data.

Table S2. Hydrogen bonds in compounds **1** to **8triclinic**.

Compound	Donor···acceptor	Description	Distance [Å]
trans-[Zn(quin)$_2$(pipe)$_2$]·2CH$_3$CN (**1**)	N2···O12[*x*, –1+*y*, *z*]	NH(pipe)···COO$^-$	3.0093(19)
[Zn(quin)$_2$(pipe)]·*cis*-[Zn(quin)$_2$(pipe)$_2$] (**2**)	N3···O22[*x*, 1.5–*y*, –0.5+*z*]	NH(pipe)···COO$^-$	2.808(2)
	N6···O52[–*x*, 1–*y*, –*z*]	NH(pipe)···COO$^-$	2.943(3)
pipeH[Zn(quin)$_3$]·CH$_3$CN (**3**)	N4···O22	NH$_2^+$(pipeH$^+$)···COO$^-$	2.807(2)
	N4···O31[1–*x*, 1–*y*, 1–*z*]	NH$_2^+$(pipeH$^+$)···COO$^-$(coordinated O)	3.045(2)
	N4···O32[1–*x*, 1–*y*, 1–*z*]	NH$_2^+$(pipeH$^+$)···COO$^-$	2.814(2)
[Zn(quin)$_2$(pipeam)]·CH$_3$CN (**4a**)	N32···O12[1+*x*, *y*, *z*]	NH(pipeam)···COO$^-$	2.9728(19)
[Zn(quin)$_2$(pipeam)]·2CHCl$_3$ (**4b**)	N32···O12[–*x*, –*y*, –*z*]	NH(pipeam)···COO$^-$	3.023(2)
pipeamH[Zn(quin)$_3$] (**5**)	N42···O32	NH$_2^+$(pipeamH$^+$)···COO$^-$	2.8473(18)
	N42···O21[1+*x*, *y*, *z*]	NH$_2^+$(pipeamH$^+$)···COO$^-$(coordinated O)	3.0342(18)
	N42···N2[1+*x*, *y*, *z*]	NH$_2^+$(pipeamH$^+$)···non-coordinated N of quin$^-$	2.9645(19)
pipeamH[Zn(quin)$_2$(CH$_3$COO)]·acetamide (**6**)	N5···O12	NH$_2$(acetamide)···COO$^-$	2.885(2)
	N5···O5[0.5–*x*, 0.5+*y*, 0.5–*z*]	NH$_2$(acetamide)···C=O(acetamide)	2.886(3)
	N32···O42	NH$_2^+$(pipeamH$^+$)···acetate	2.862(2)
	N32···O21[*x*, 1+*y*, *z*]	NH$_2^+$(pipeamH$^+$)··· COO$^-$(coordinated O)	2.981(2)
pyroH[Zn(quin)$_3$]·CH$_3$CN (**8monoclinic**)	N4···O22	NH$_2^+$(pyroH$^+$)···COO$^-$	2.776(4)
	N4···O32[1–*x*, 1–*y*, 1–*z*]	NH$_2^+$(pyroH$^+$)···COO$^-$	2.772(3)
pyroH[Zn(quin)$_3$]·CH$_3$CN (**8triclinic**)	N4···O21[–1+*x*, *y*, *z*]	NH$_2^+$(pyroH$^+$)···COO$^-$(coordinated O)	2.926(3)
	N4···O32	NH$_2^+$(pyroH$^+$)···COO$^-$	2.777(3)

Table S3. Hydrogen bonds in compounds **9** to **13**.

Compound	Donor···acceptor	Description	Distance [Å]
pyroH[Zn(quin)$_2$Cl] (**9**)	N2···O12	NH_2^+(pyroH$^+$)···COO^-	2.725(2)
[Zn(quin)$_2$(pyroam)]·CH_3CN·0.5pyroam·0.5H_2O (**10a**)	N32···O22[1+*x*, *y*, *z*]	NH(pyroam)···COO^-	3.011(2)
	O5···O12[2–*x*, 1–*y*, –*z*]	OH(H_2O)···COO^-	2.825(4)
	O5···N52	OH(H_2O)···NH(pyroam)	2.853(7)
[Zn(quin)$_2$(pyroam)]·2$CHCl_3$ (**10b**)	N32···O12[2–*x*, 1–*y*, 1–*z*]	NH(pyroam)···COO^-	3.022(3)
[Zn(quin)$_2$(pyroam)]·CH_2Cl_2 (**10c**)	N32···O22[1+*x*, *y*, *z*]	NH(pyroam)···COO^-	3.038(2)
pyroamH[Zn(quin)$_3$] (**11monoclinic**)	N42···O12	NH_2^+(pyroamH$^+$)···COO^-	2.930(5)
	N42···O22[1+*x*, *y*, *z*]	NH_2^+(pyroamH$^+$)···COO^-	2.961(5)
pyroamH[Zn(quin)$_3$] (**11triclinic**)	N42···N3[1+*x*, *y*, *z*]	NH_2^+(pyroamH$^+$)···non-coordinated N of $quin^-$	2.996(14)
	N42···O22	NH_2^+(pyroamH$^+$)···COO^-	2.890(14)
trans-[Zn(quin)$_2$(morph)$_2$] (**12**)	N3···O22	NH(morph)···COO^-	2.914(2)
	N4···O12[*x*, *y*, 1+*z*]	NH(morph)···COO^-	2.944(2)
morphH[Zn(quin)$_3$]·CH_3CN (**13**)	N4···O31[1–*x*, 1–*y*, 1–*z*]	NH_2^+(morphH$^+$)···COO^-(coordinated O)	2.924(3)
	N4···O32[1–*x*, 1–*y*, 1–*z*]	NH_2^+(morphH$^+$)···COO^-	2.898(3)
	N4···O22	NH_2^+(morphH$^+$)···COO^-	2.828(4)
	N4···O21	NH_2^+(morphH$^+$)···COO^-(coordinated O)	3.068(3)

Figure S5. Hydrogen bonding in *trans*-[Zn(quin)$_2$(pipe)$_2$]·2CH$_3$CN (**1**). The N–H···COO$^-$ bonds link the *trans*-[Zn(quin)$_2$(pipe)] molecules into chains that run along *b*-axis. Each chain may be alternatively described as an infinite repetition of a cyclic motif, labelled $R_2^2(12)$ in graph set notation.[S2] The chains pack forming channels that are filled with solvent molecules of acetonitrile. Volume of the channels *per* unit cell is 206.4 Å^3 and represents 14.1 % of the total volume.[S3]

(i) Section of a chain.

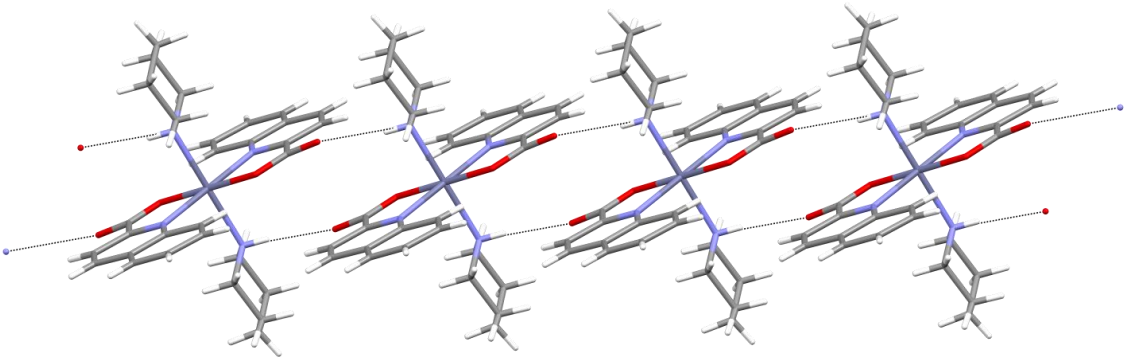

(ii) A view along channels.

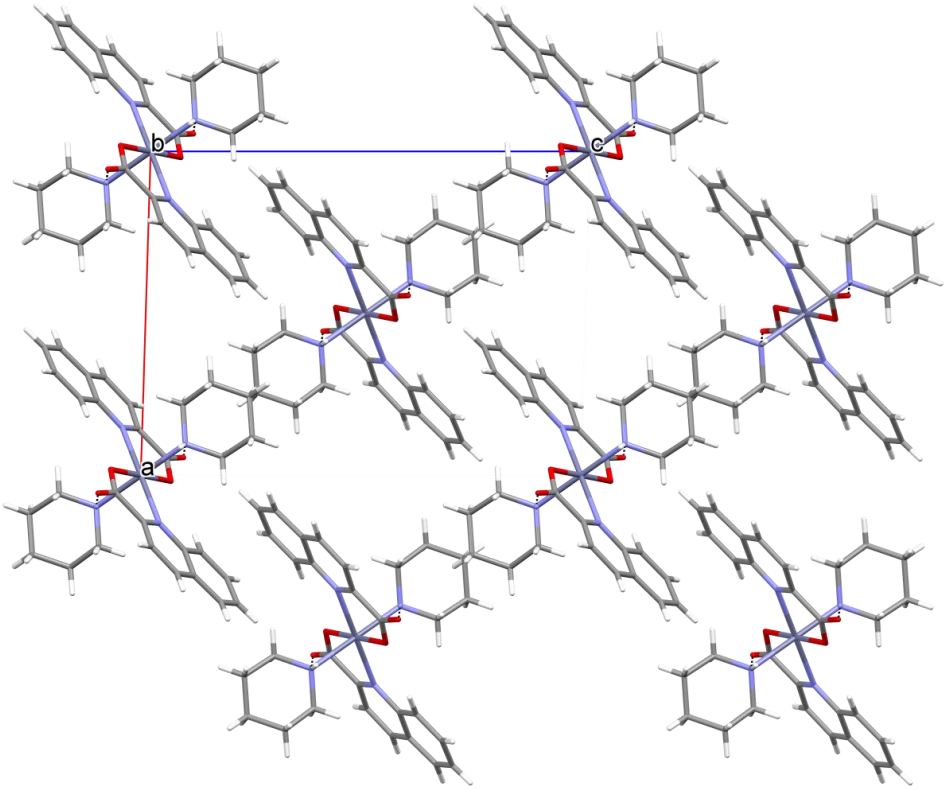

Figure S6. Hydrogen bonding in pipeH[Zn(quin)$_3$]·CH$_3$CN (**3**): N–H···COO$^-$ bonds link pipeH$^+$ and [Zn(quin)$_3$]$^-$ ions into rings, denoted as $R_4^4(20)$.[S2]

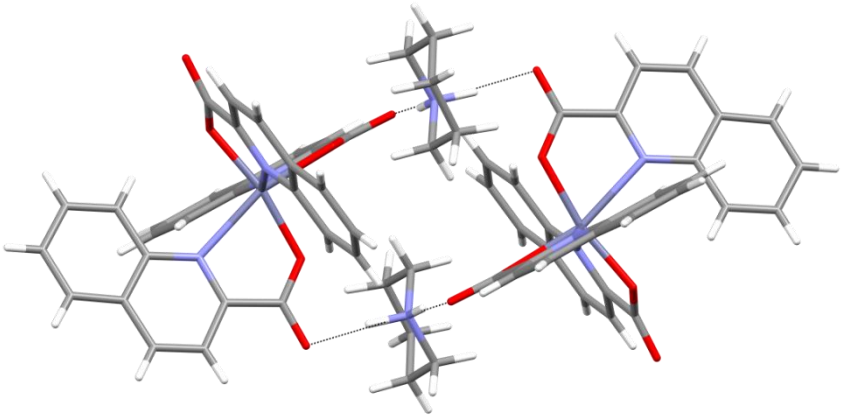

Figure S7. Hydrogen bonding in [Zn(quin)$_2$(pipeam)]·CH$_3$CN (**4a**): (i) the N–H(pipeam)···COO$^-$ bonds link the [Zn(quin)$_2$(pipeam)] molecules into chains, (ii) the chains pack with the formation of channels that run along *a*-axis.

(i)

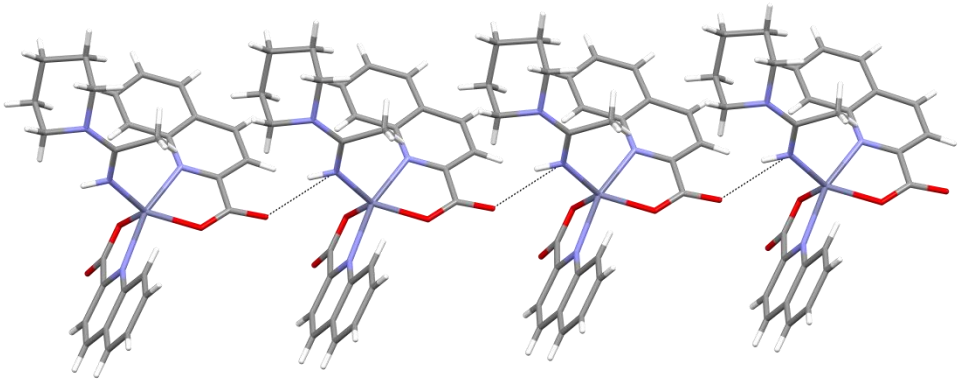

(ii)

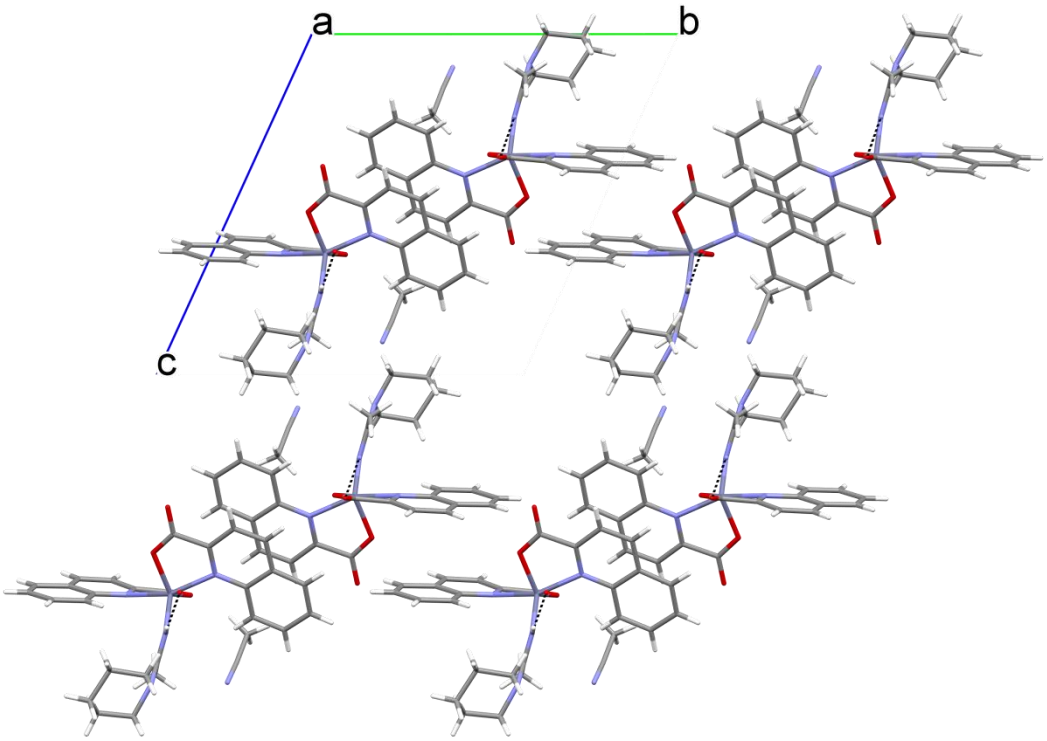

Figure S8. A view along the channels in [Zn(quin)$_2$(pipeam)]·CH$_3$CN (**4a**). Acetonitrile molecules are not shown.

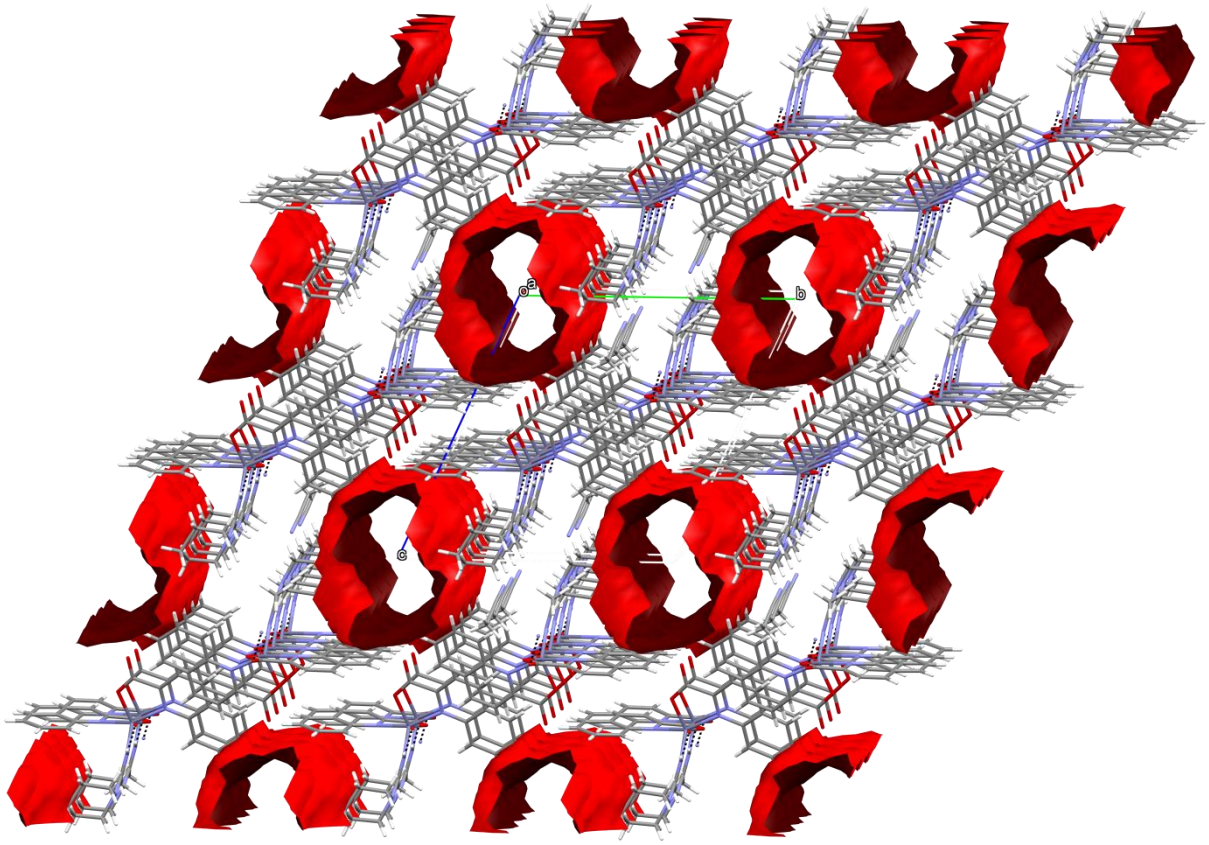

Figure S9. Hydrogen bonding in $[Zn(quin)_2(pipeam)]\cdot 2CHCl_3$ (**4b**): complex molecules are linked *via* N–H(pipeam)···COO^- interactions into dimers.

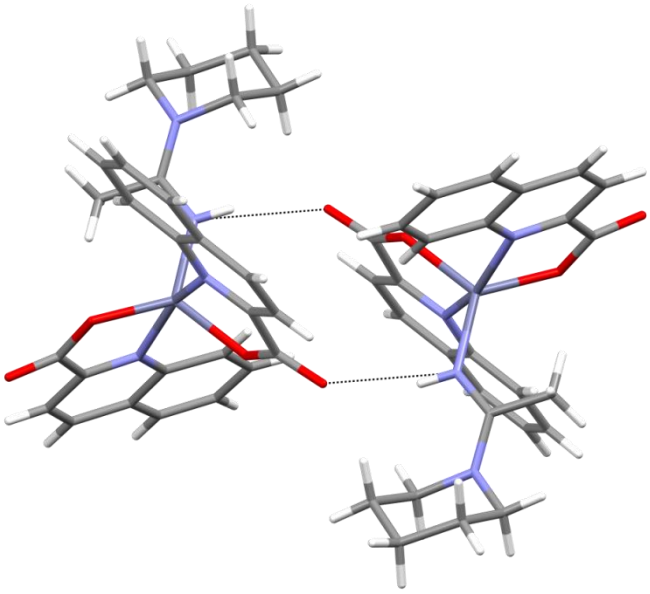

Figure S10. Hydrogen bonding in pipeamH[Zn(quin)$_3$] (**5**): the protonated amidine forms three hydrogen bonds with two [Zn(quin)$_3$]$^-$ anions. As a result, infinite chains are formed that run along *a*-axis.

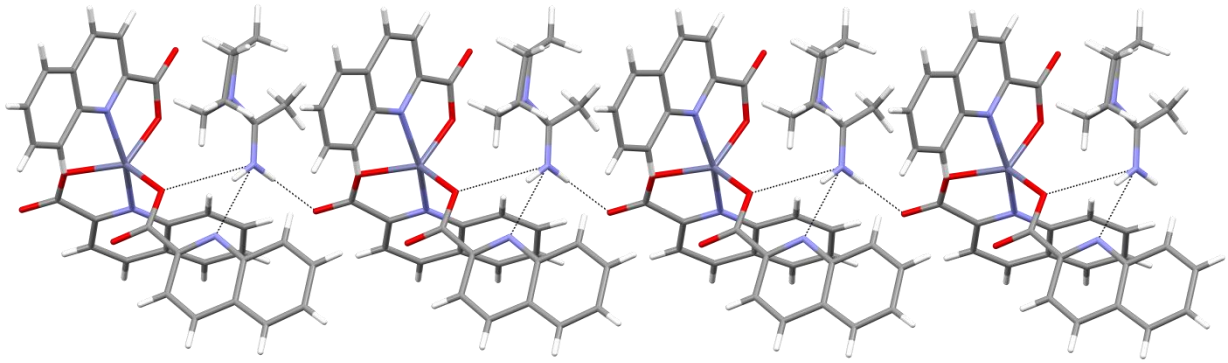

Figure S11. Hydrogen bonding in pipeamH[Zn(quin)$_2$(CH$_3$COO)]·acetamide (**6**): section of a chain that runs along *b*-axis. The overall pattern consists of a central chain of H-bonded acetamide molecules (colored green) with appended [Zn(quin)$_2$(CH$_3$COO)]$^-$ anions (light grey) and pipeamH$^+$ cations (orange) to its sides.

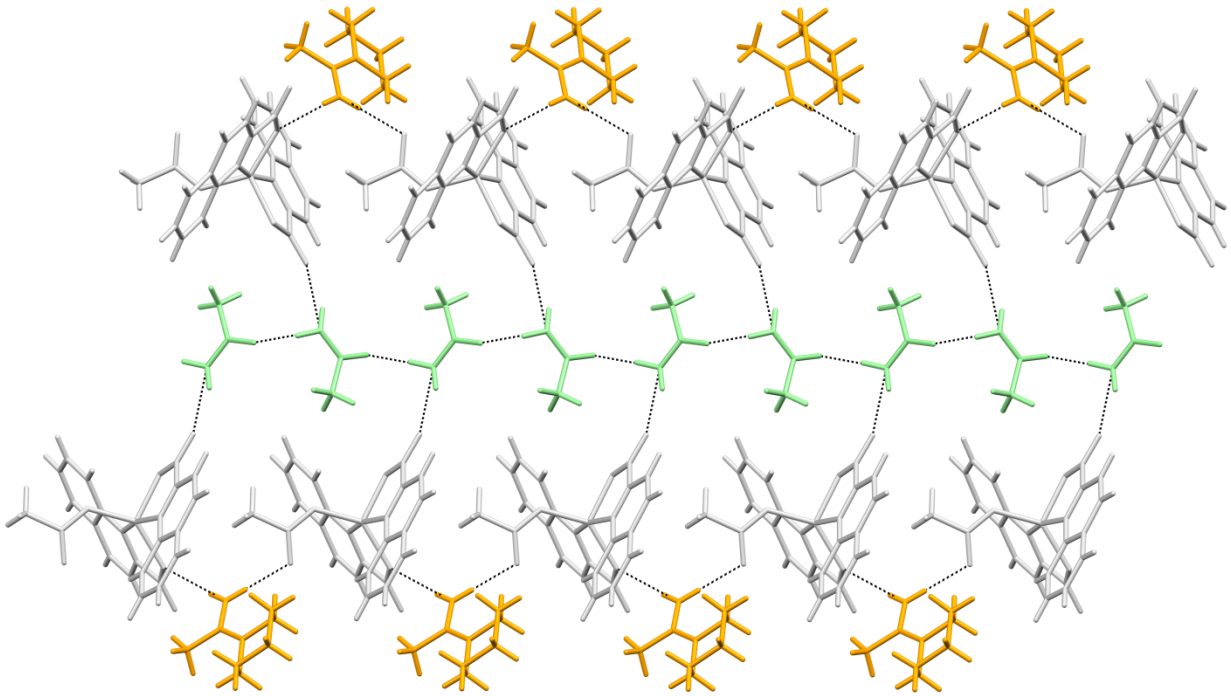

Figure S12. Hydrogen bonding in pyroH[Zn(quin)$_2$Cl] (**9**): N–H···COO$^-$ bonds link pyroH$^+$ and [Zn(quin)$_2$Cl]$^-$ ions into chains. The chains run along *a*-axis.

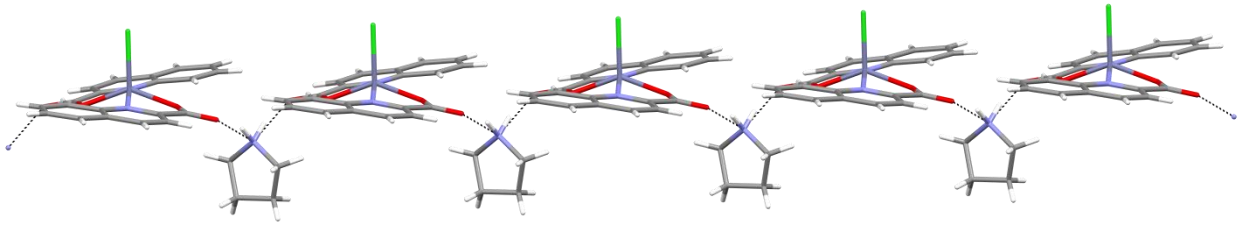

Figure S13. Hydrogen bonding in [Zn(quin)$_2$(pyroam)]·CH$_3$CN·0.5pyroam·0.5H$_2$O (**10a**). The N–H(amidine)···COO$^-$ hydrogen bonds link complex molecules into infinite chains that run along *a*-axis. The other carboxylate moiety is H-bonded to a water molecule that is bonded also to a non-coordinated amidine. Chains with appended water and amidine molecules (neither are shown) pack in a parallel fashion. Color code: light grey - complex molecules, orange - acetonitrile.

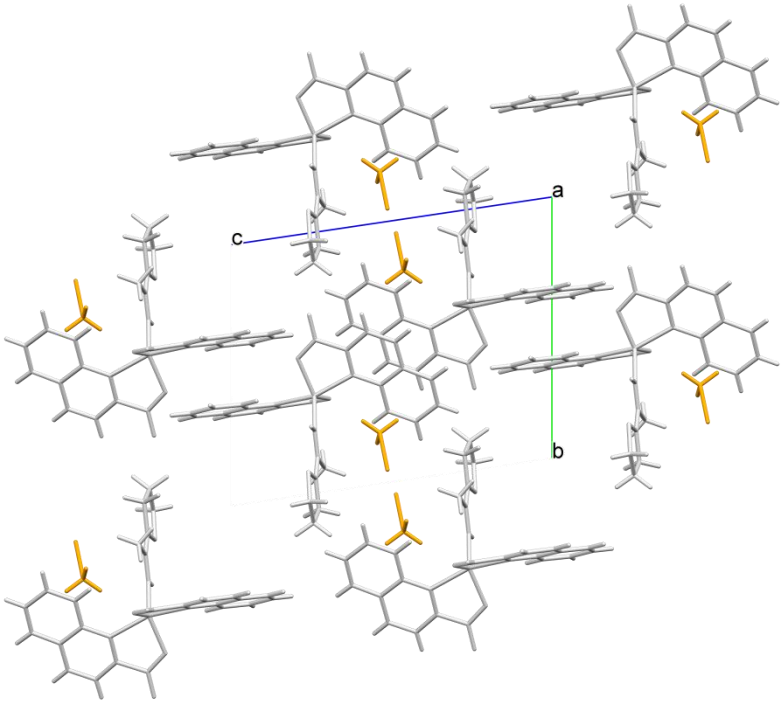

Figure S14. Hydrogen bonding in $[Zn(quin)_2(pyroam)]\cdot 2CHCl_3$ (**10b**): a pair of N–H···COO^- hydrogen bonds links complex molecules into dimers.

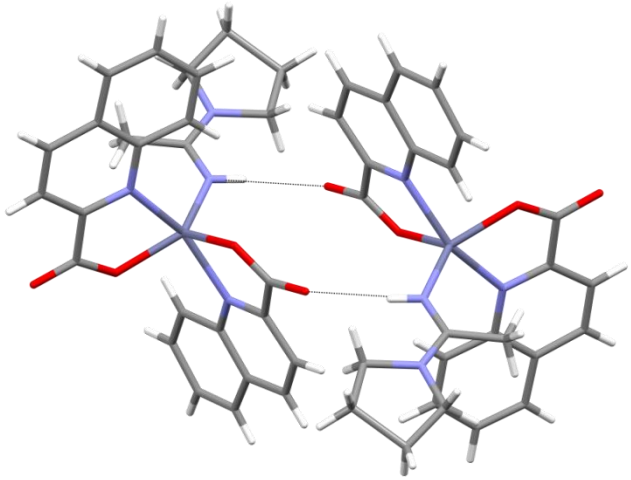

Figure S15. Hydrogen bonding in $[Zn(quin)_2(pyroam)]\cdot CH_2Cl_2$ (**10c**): (i) N–H(amidine)···COO^- hydrogen bonds link molecules into chains, and (ii) the chains of H-bonded complex molecules pack with the formation of channels that run along *a*-axis. The CH_2Cl_2 molecules, accommodated in these channels, are not shown.

(i)

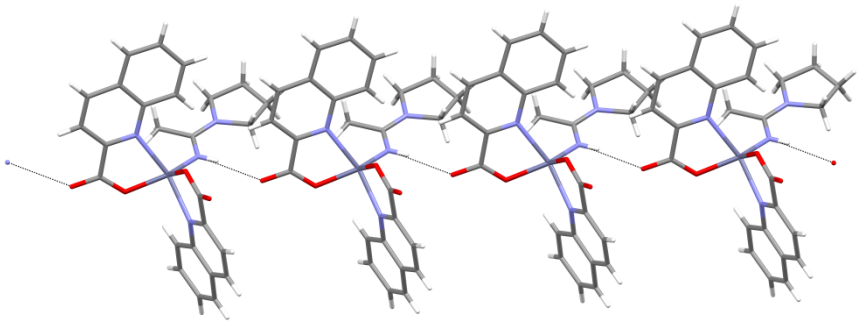

(ii)

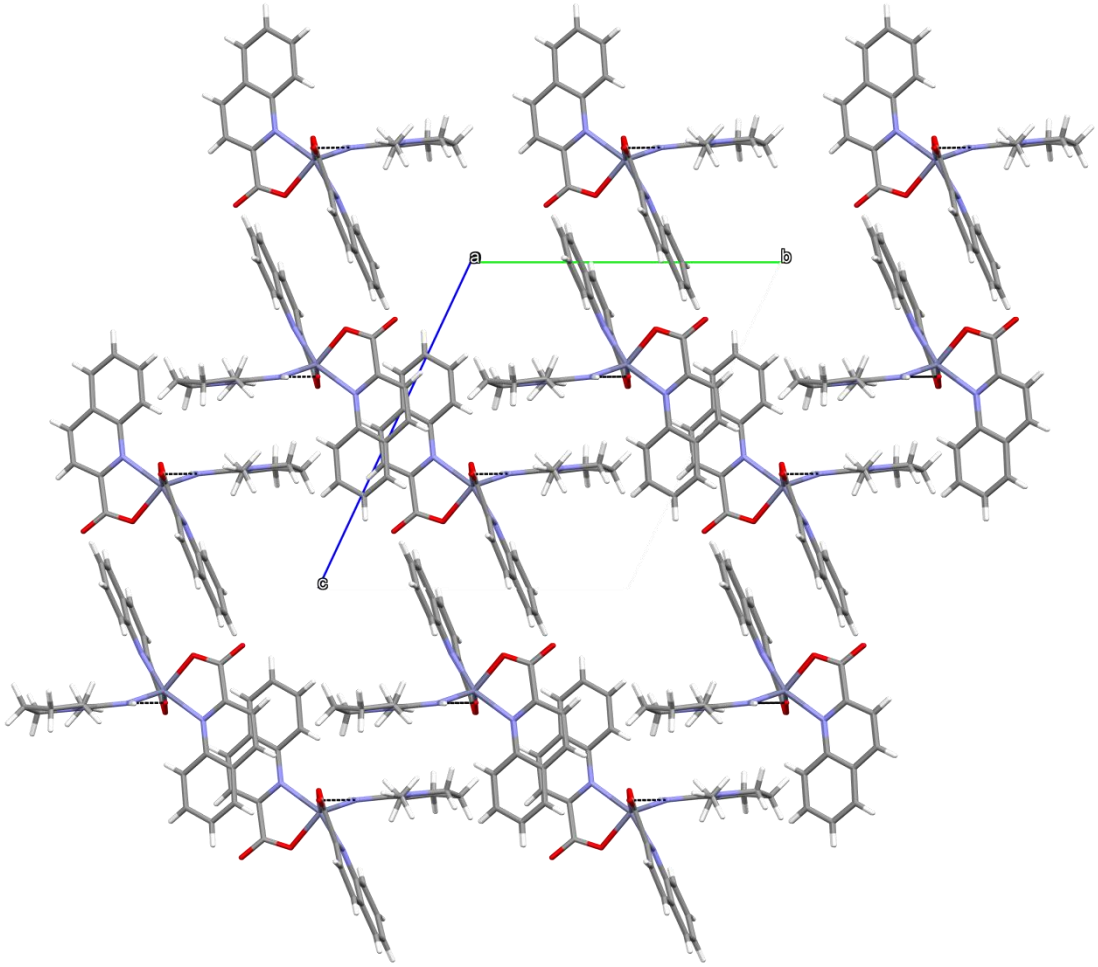

Figure S16. Hydrogen bonding in *trans*-[Zn(quin)$_2$(morph)$_2$] (**12**): N–H···COO$^-$ bonds link complex molecules into chains that run along *c*-axis.

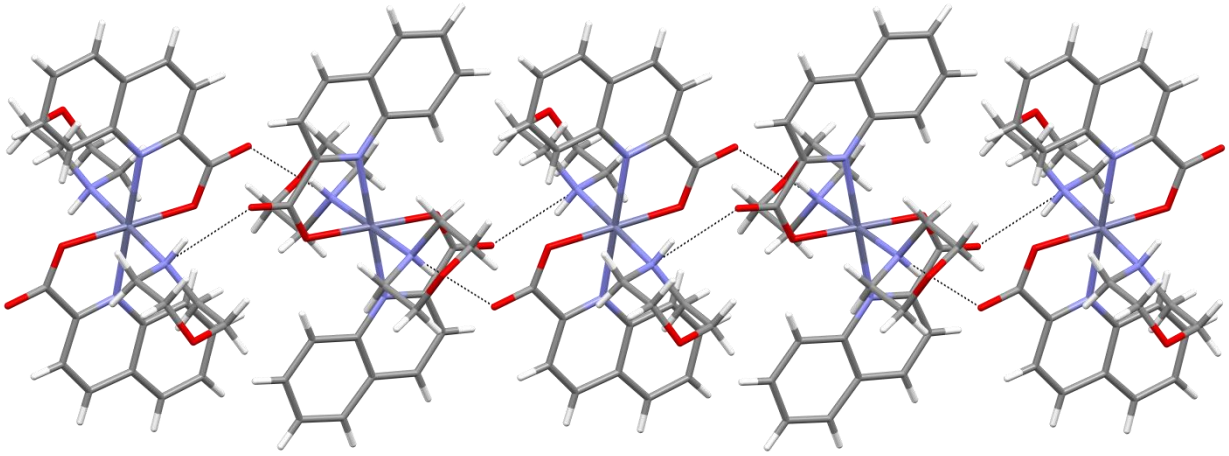

2. DFT calculations on pyroamH[Zn(quin)$_3$] (11) polymorphs

DFT optimized geometries of **6-[Zn(quin)$_3$]$^-$** and **5-[Zn(quin)$_3$]$^-$** in bulk acetonitrile are in good agreement with their solid state structures, determined by X-ray analysis on single crystals. For both, we also optimized molecular geometries of short chain segments, each consisting of two pyroamH$^+$ countercations and a corresponding [Zn(quin)$_3$]$^-$ anion, and compared their energies. These segments were labelled as **11triclinic_5_chain** and **11monoclinic_6_chain**. The **5-[Zn(quin)$_3$]$^-$** complex is 5.6 kcal·mol^{-1} less stable than **6-[Zn(quin)$_3$]$^-$**. This is also true for the chain segments with the pyroamH$^+$ cations: **11triclinic_5_chain** is 2.02 kcal·mol^{-1} higher in energy than **11monoclinic_6_chain**. These small energy differences are consistent with the experimental observations. In addition, the optimized geometries of **11monoclinic_6_chain** and **11triclinic_5_chain** retain the hydrogen bond suggested by the X-ray analysis with a H···O distance of 1.87/1.98 Å and a N–H···O angle of 160.9/171.6°. This hydrogen bond was confirmed by AIM analysis of the electron density, which yielded a bond critical point (**11monoclinic**: ρ_{bcp} = +0.041 e$^-$/Bohr^3; $\nabla^2\rho_{bcp}$ = +0.012 e$^-$/Bohr^5; **11triclinic**: +0.0248 e$^-$/Bohr^3; $\nabla^2\rho_{bcp}$ = +0.065 e$^-$/Bohr^5) and bond paths connecting the N–H and O atoms

Figure S17. Bond critical points (bcps, blue dots) and bond paths connecting the N–H and O functionalities in the **11triclinic_5_chain** (left) and the **11monoclinic_6_chain** (right) segments. The bcps and paths are superimposed of the Laplacian of the electron density ($\nabla^2\rho$; solid red trace and dashed blue trace for positive and negative values respectively).

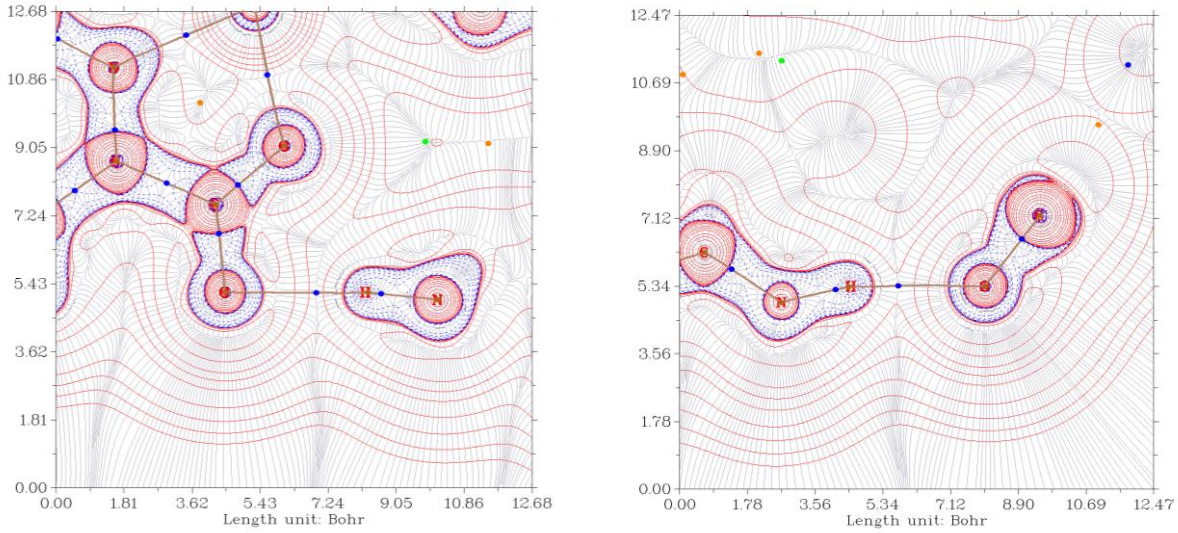

The Pointcaré-Hopf relationship was satisfied in the topological analysis.

Figure S18. Relaxed Potential Energy Surface (PES) Scan of the $[Zn(quin)_3]^-$ anion along the N···Zn coordinate. Starting from the right-hand side, **5-[Zn(quin)$_3$]$^-$** evolves to a local minimum, **5b-[Zn(quin)$_3$]$^-$**, featuring a $\pi\cdots\pi$ stacking between two quinaldinates. Further shortening of the N–Zn distance yields **6-[Zn(quin)$_3$]$^-$**, the most stable isomer.

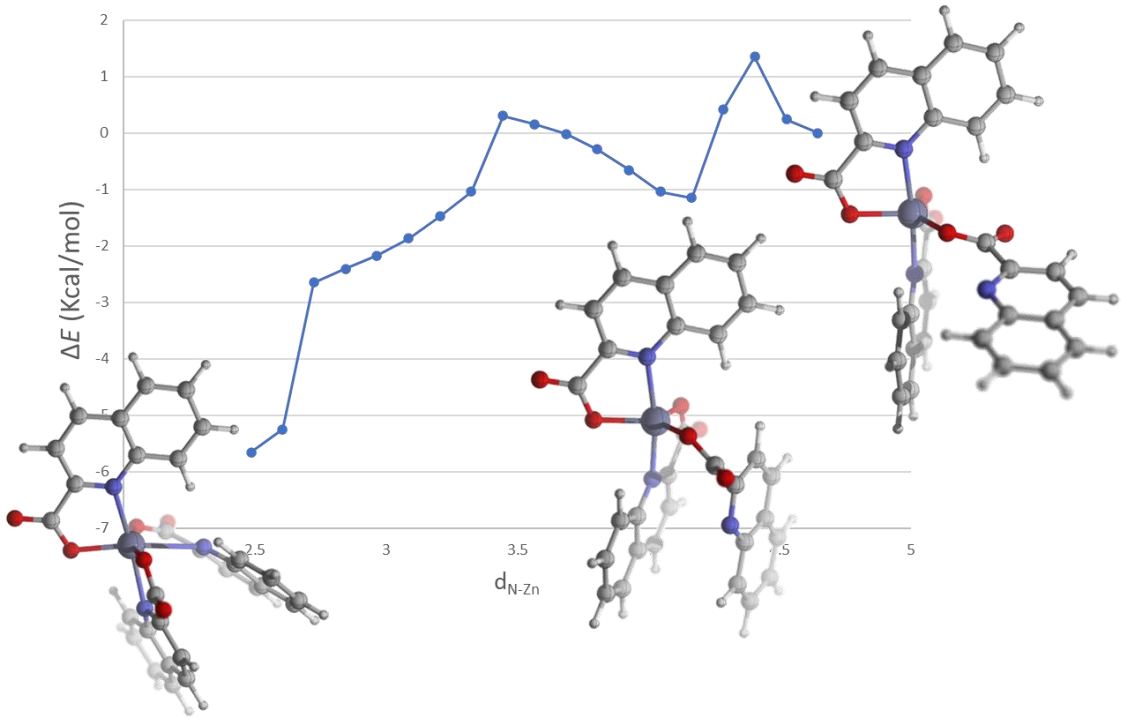

The vertical axis in the above figure (Figure S18) corresponds to electronic energy in acetonitrile for the constrained ($d_{N\text{-}Zn}$ distances are fixed for every step of the scan) geometries of the $[Zn(quin)_3]^-$ anion. The local minimum in the PES scan profile was the freely optimized to yield **5b-[Zn(quin)$_3$]$^-$** and the optimized structure was confirmed as a minimum with vibrational analysis (all frequencies are positive). The relative energies reported in the main text for **5-[Zn(quin)$_3$]$^-$**, **5b-[Zn(quin)$_3$]$^-$**, **and 6-[Zn(quin)$_3$]$^-$** are zero-point energies derived from vibrational analysis.

Figure S19. Chain of two pyroamH$^+$ cations and a five-coordinate [Zn(quin)$_3$]$^-$ ion, optimized from **11triclinic_5_chain**. The blue arrow points at the N–H···O bond and the green arrows point at the region of weak attractive interactions (green surfaces), bcps and bond paths (orange traces) between the pyroamH$^+$ cations and the five-coordinate complex ions.

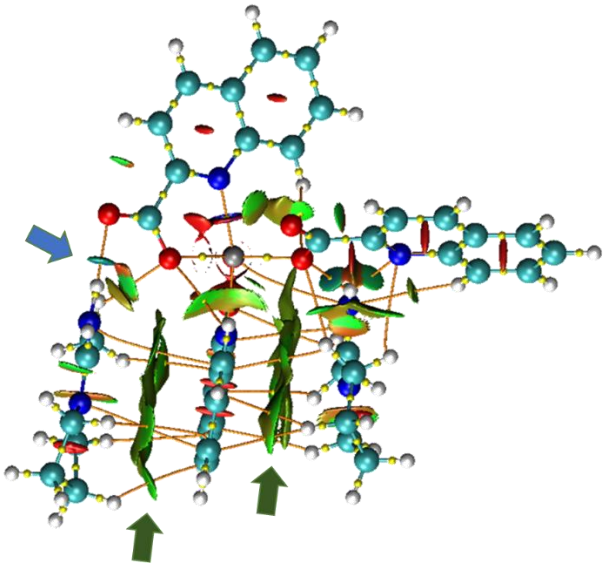

Figure S20. NCI plots, generated at the promolecular level, for portions of the frozen crystal structures of **11triclinic** and **11monoclinic**, revealing $\pi\cdots\pi$ and C–H$\cdots\pi$ interactions (green surfaces).

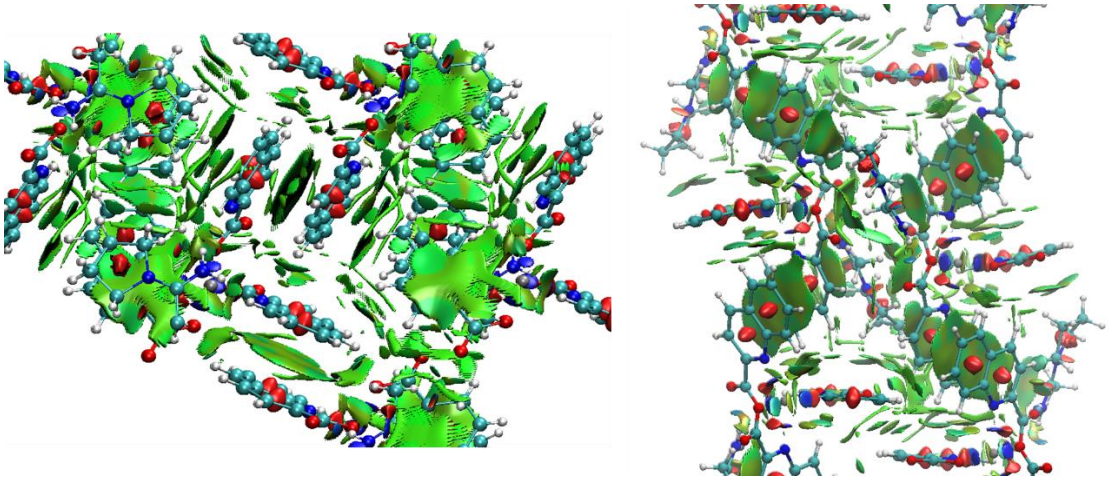

3. Detection of ammonia

Figure S21. Mass spectrometry of gaseous phases of the morpholine mixtures.

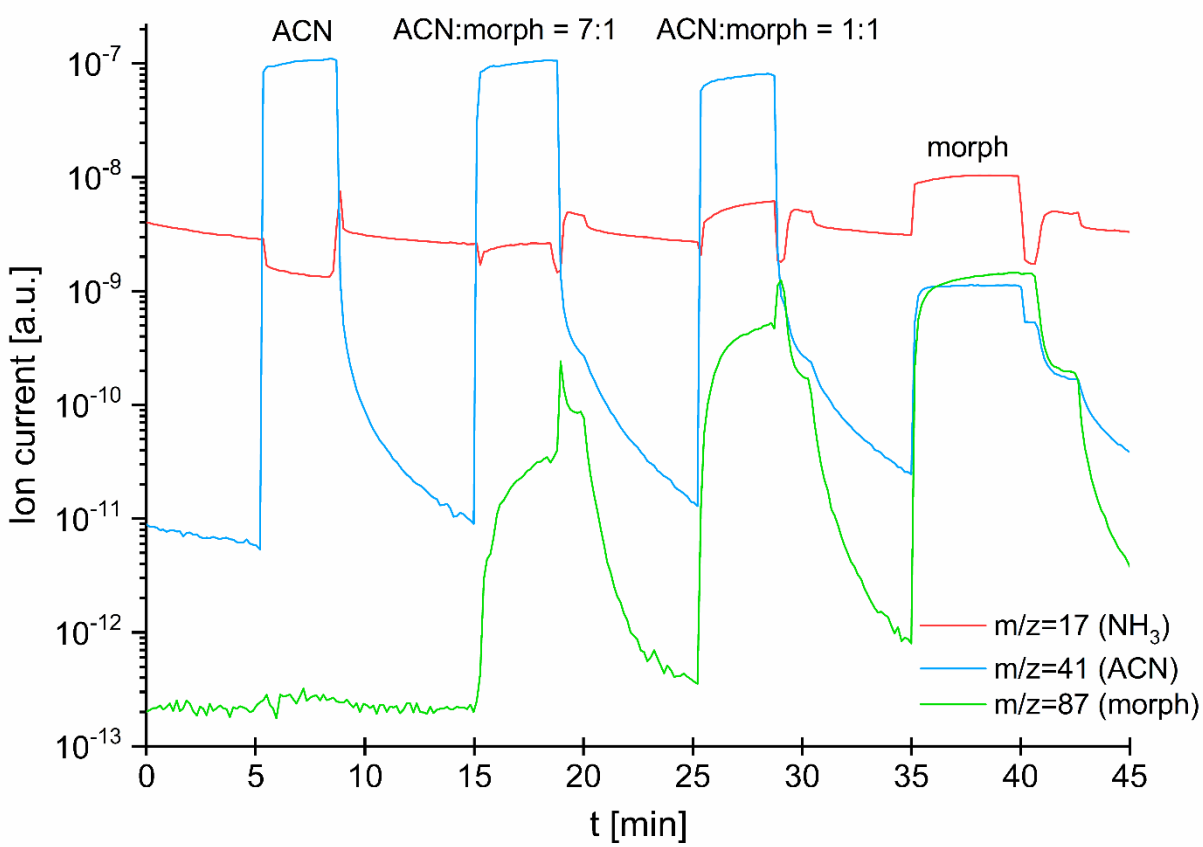

4. Infrared spectra

Figure S22. Infrared spectrum of $[Zn(quin)_2(pipe)_2]\cdot 2CH_3CN$ (**1**).

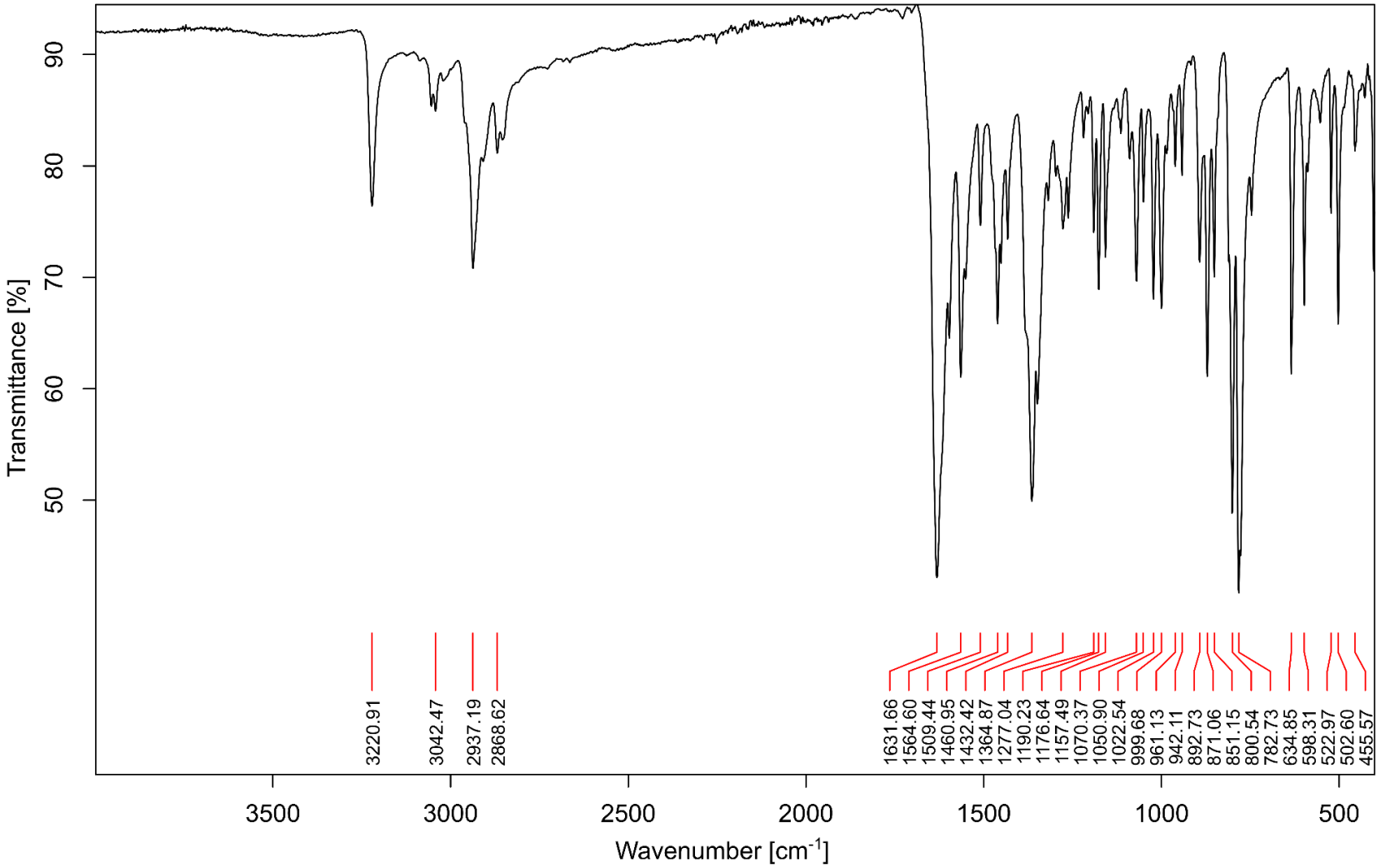

Figure S23. Infrared spectrum of [Zn(quin)$_2$(pipe)]·*cis*-[Zn(quin)$_2$(pipe)$_2$] (**2**).

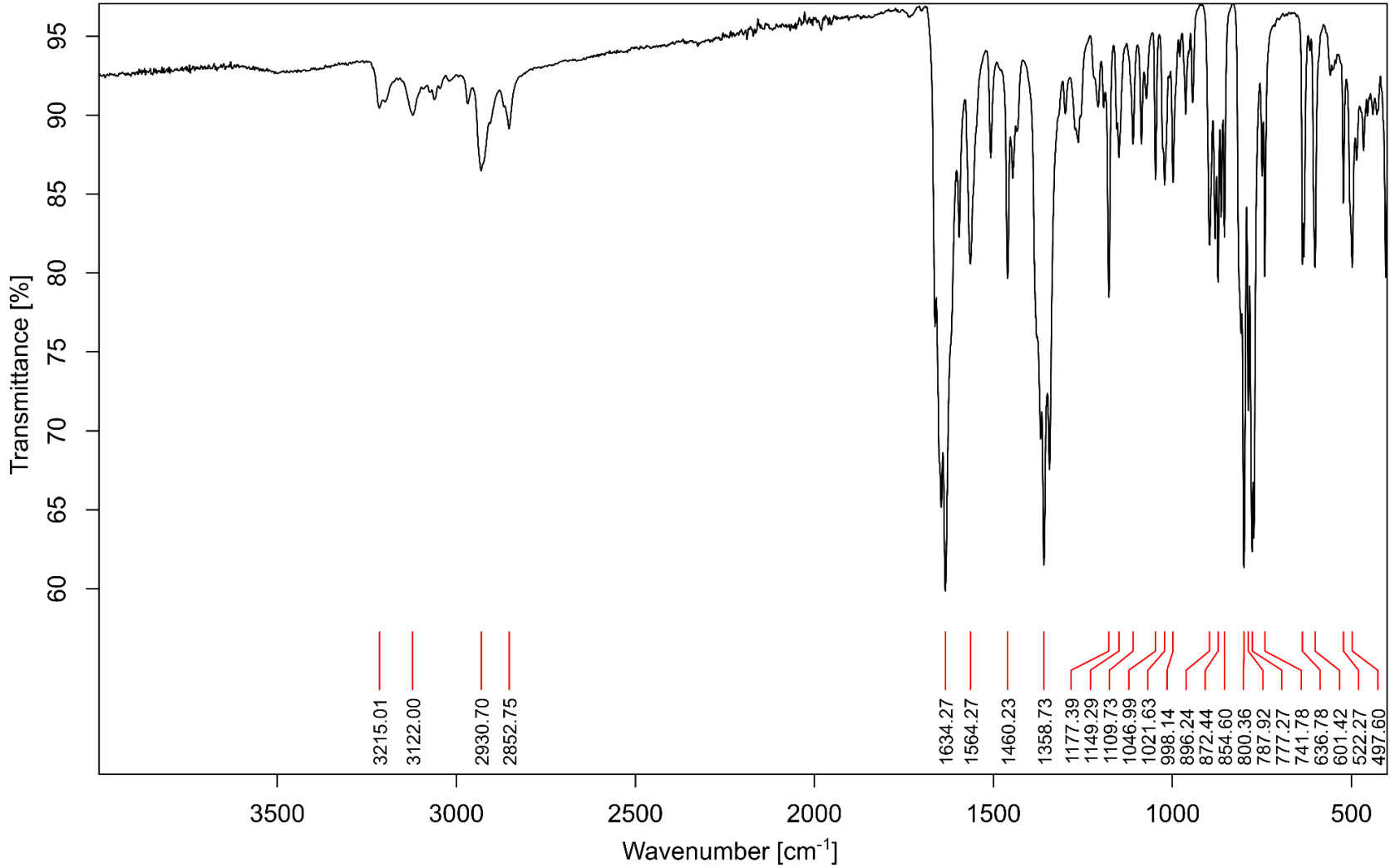

Figure S24. Infrared spectrum of pipeH[Zn(quin)$_3$]·CH_3CN (**3**).

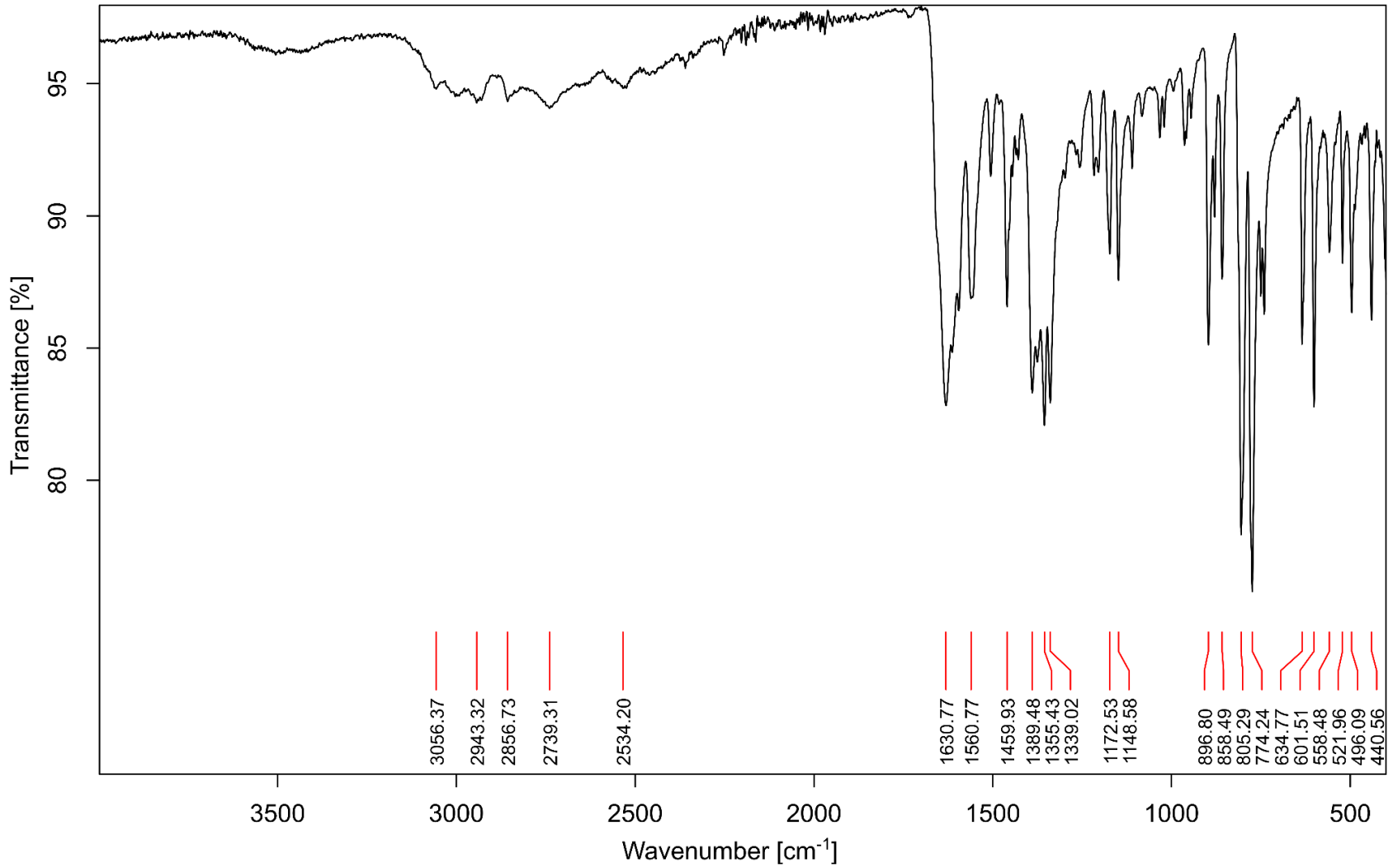

Figure S25. Infrared spectrum of $[Zn(quin)_2(pipeam)]\cdot CH_3CN$ (**4a**).

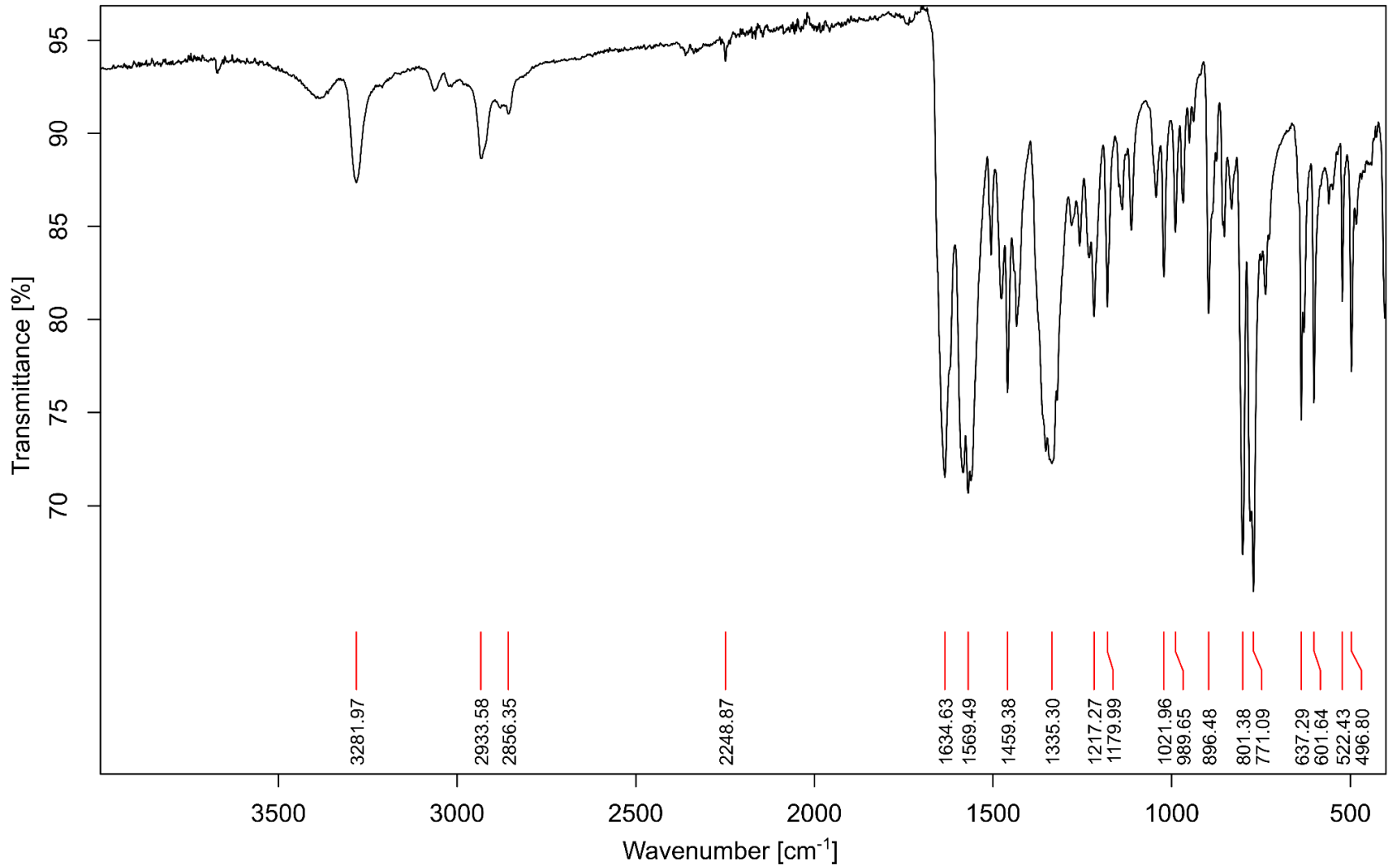

Figure S26. Infrared spectrum of $[Zn(quin)_2(pipeam)]\cdot 2CHCl_3$ (**4b**).

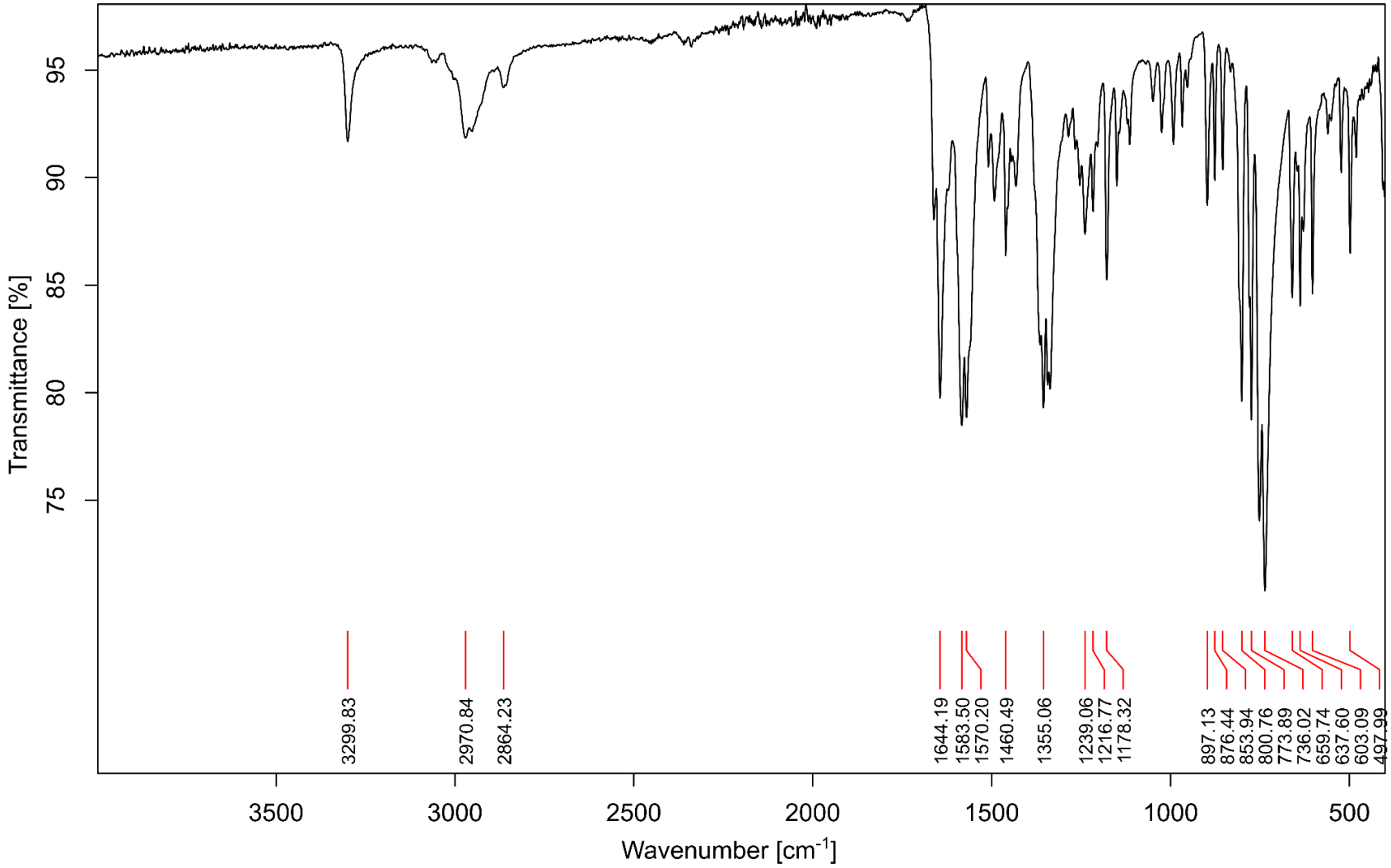

Figure S27. Infrared spectrum of pipeamH[Zn(quin)$_3$] (**5**).

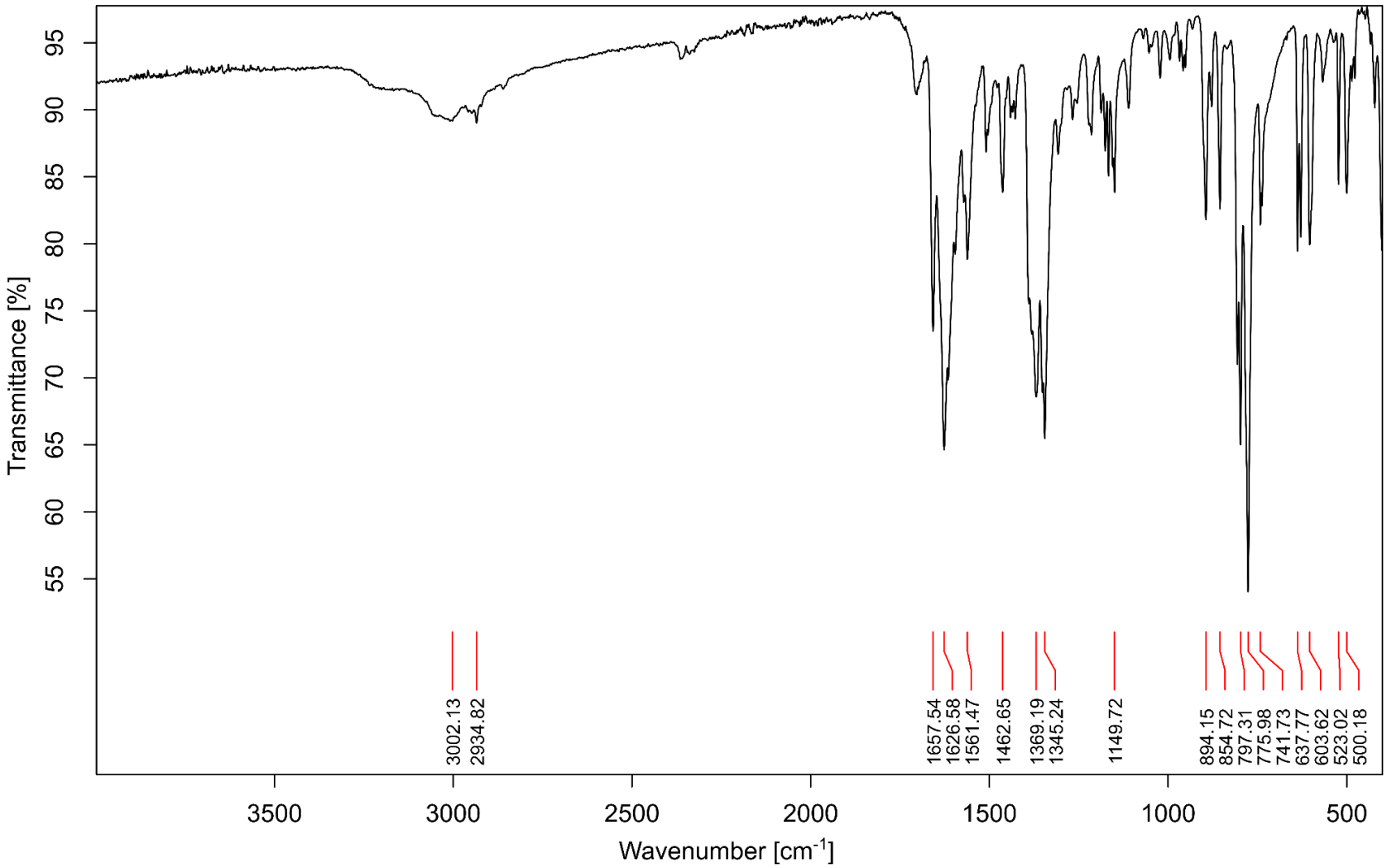

Figure S28. Infrared spectrum of $[Zn(quin)_2(pyro)_2]$ (**7**).

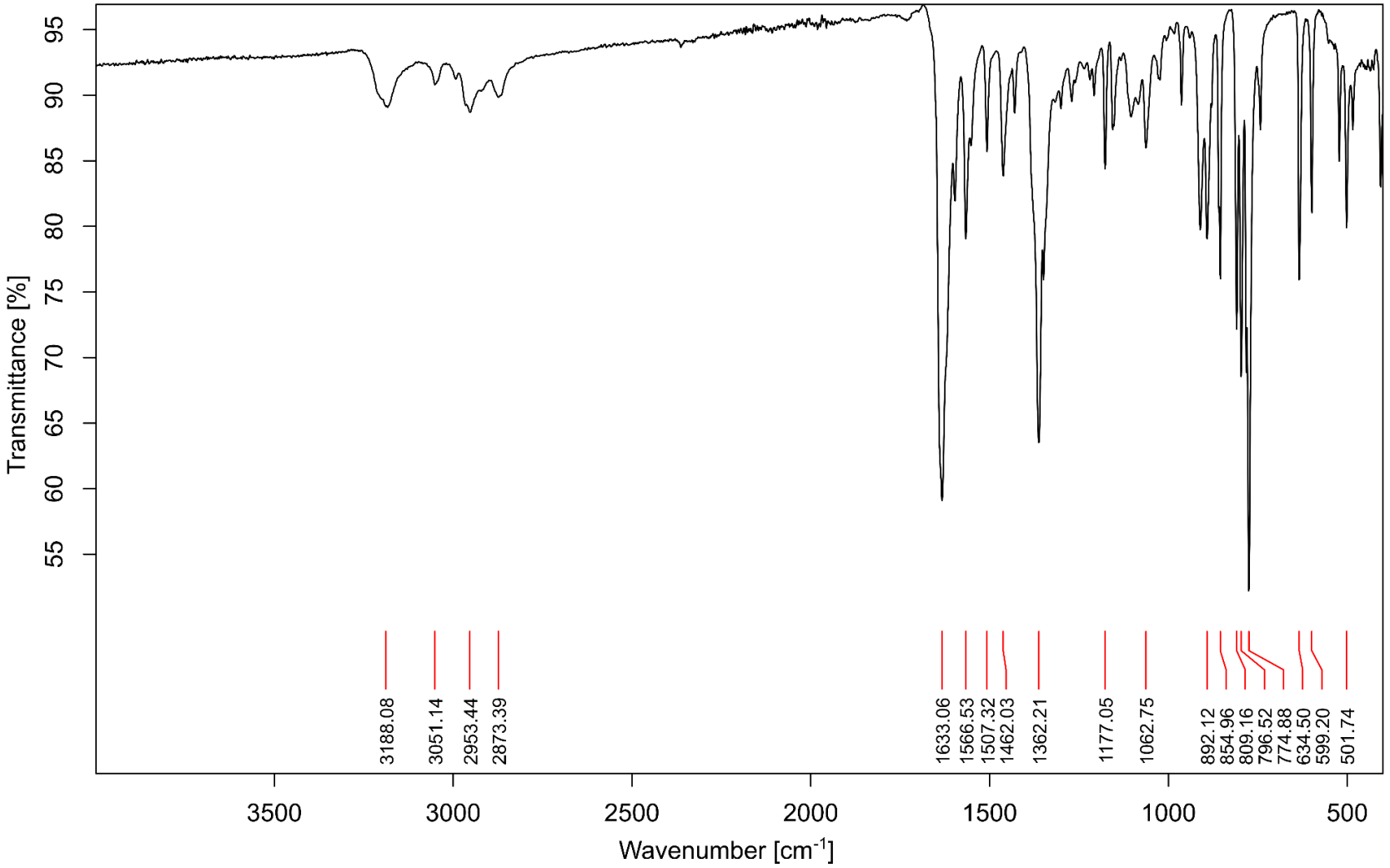

Figure S29. Infrared spectrum of pyroH[Zn(quin)$_3$]·CH_3CN (**8**).

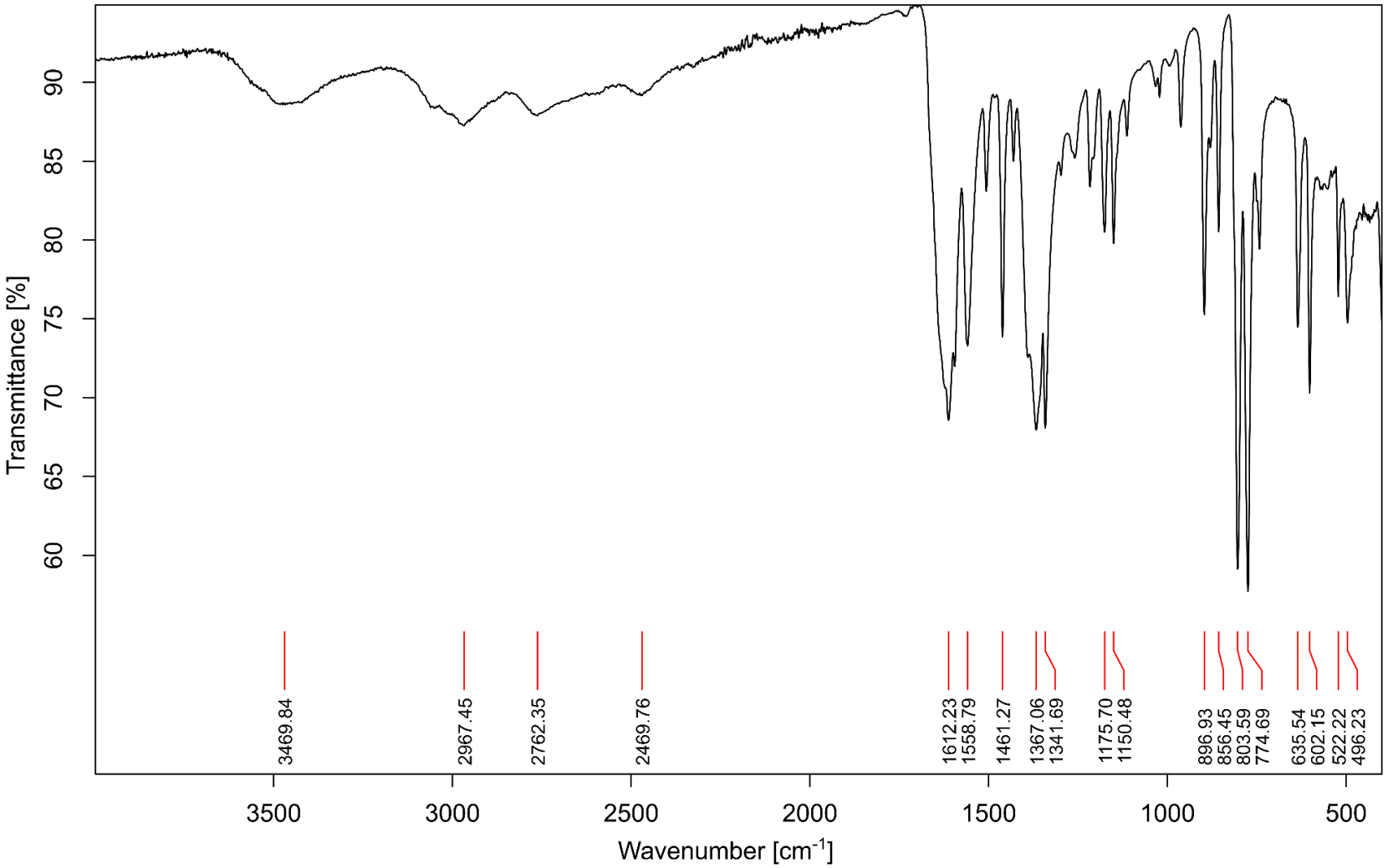

Figure S30. Infrared spectrum of pyroH[Zn(quin)$_2$Cl] (**9**).

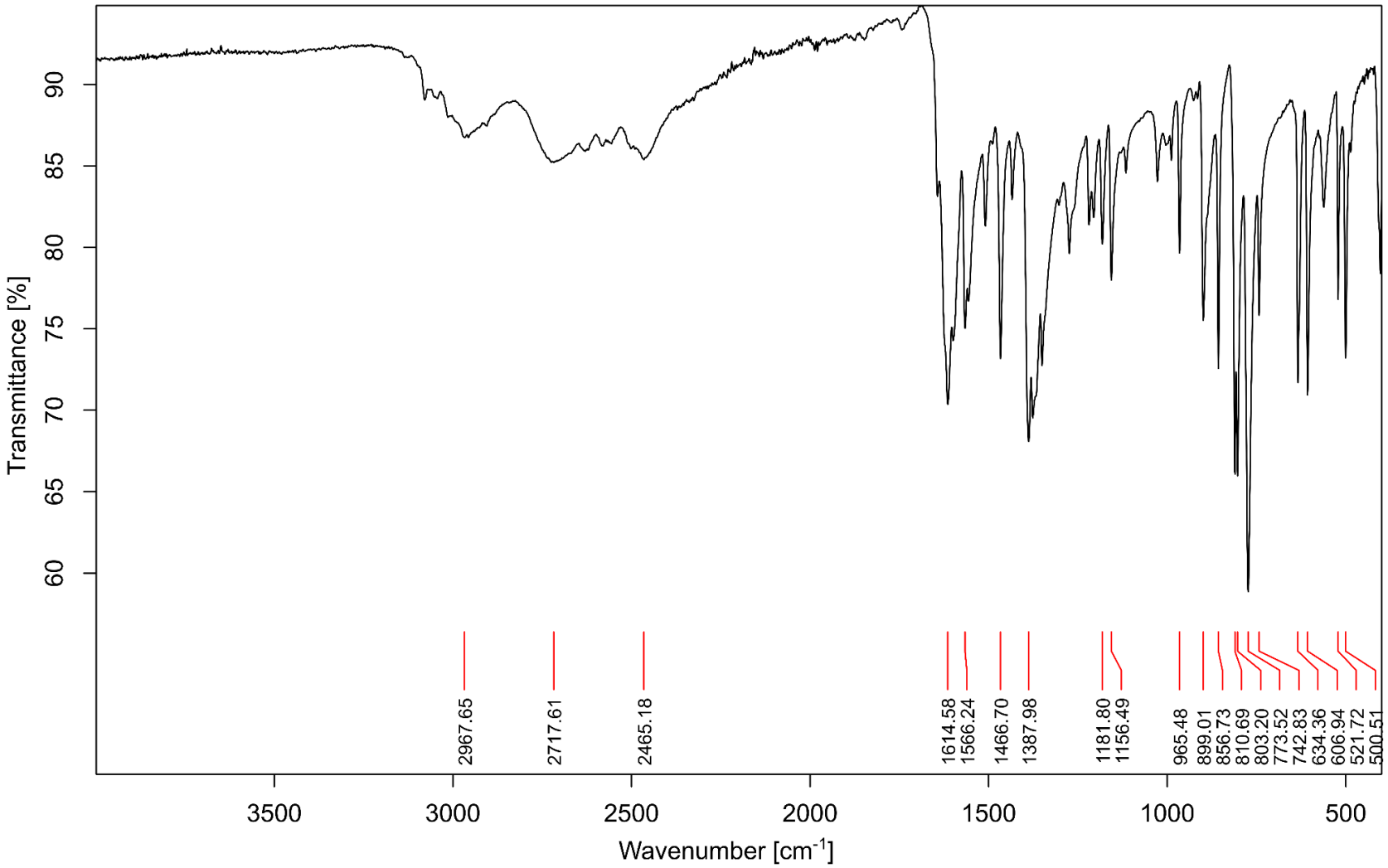

Figure S31. Infrared spectrum of [Zn(quin)$_2$(pyroam)]·CH$_3$CN·0.5pyroAm·0.5H$_2$O (**10a**).

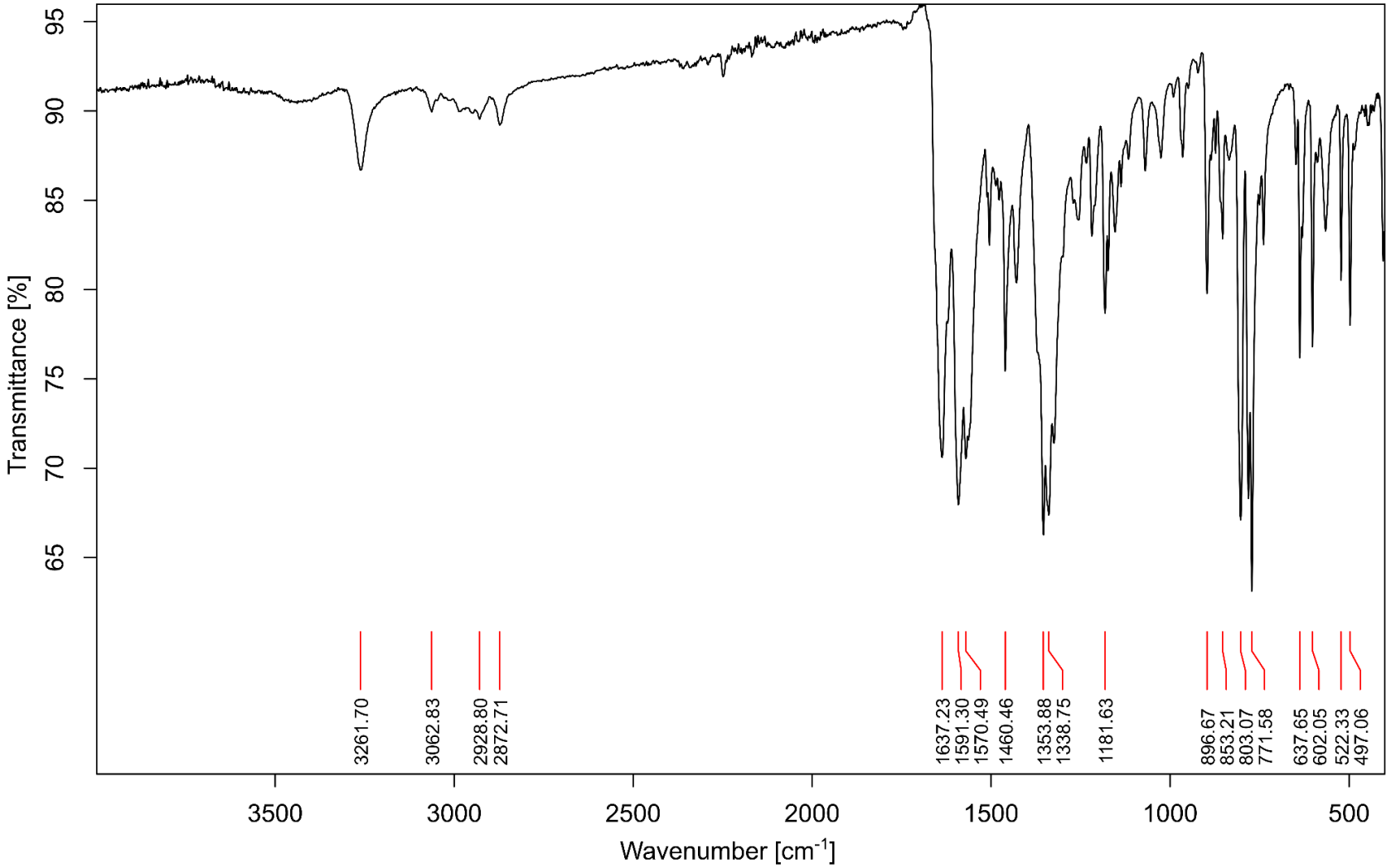

Figure S32. Infrared spectrum of $[Zn(quin)_2(pyroam)]\cdot 2CHCl_3$ (**10b**).

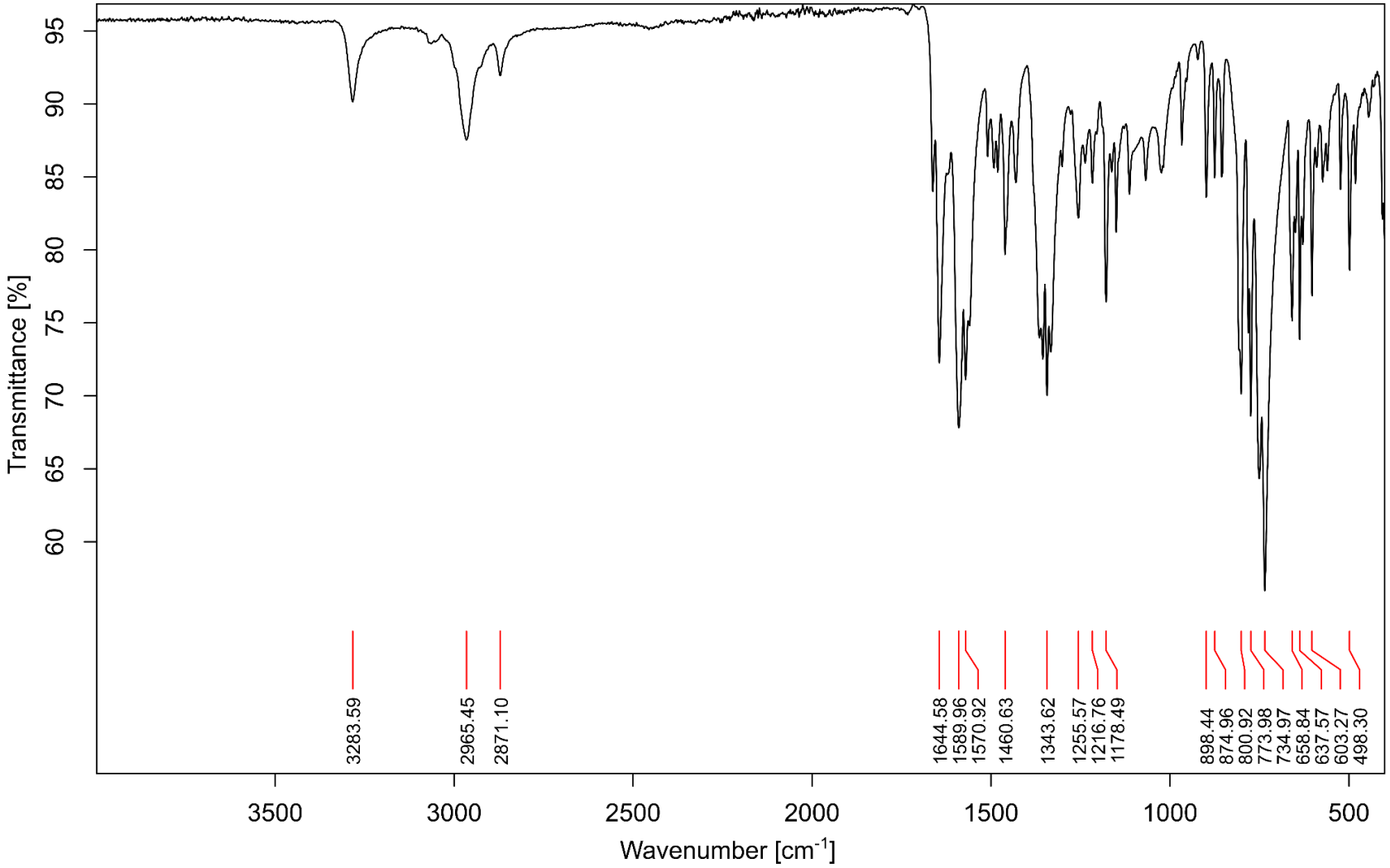

Figure S33. Infrared spectrum of pyroamH[Zn(quin)$_3$] (**11**).

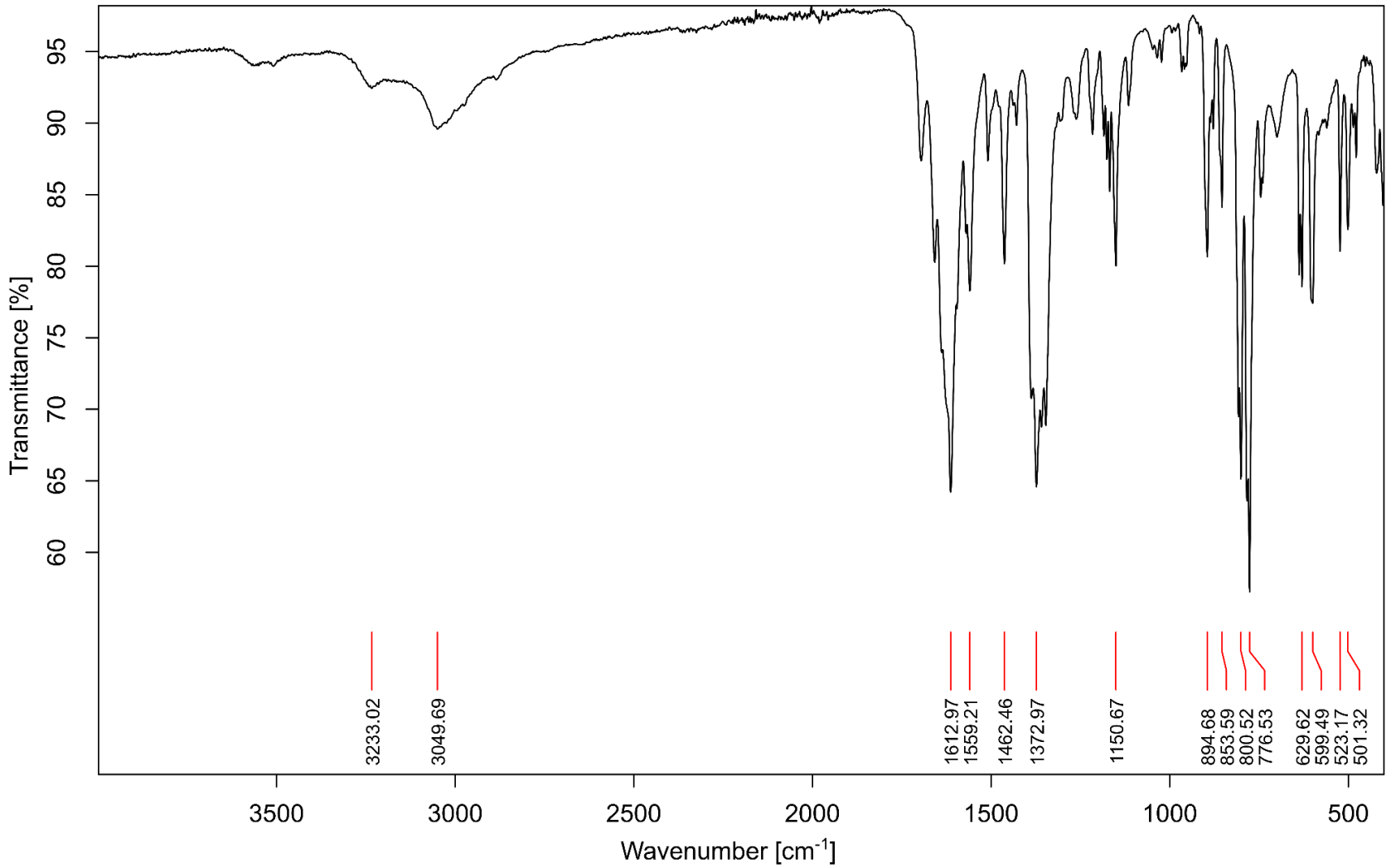

Figure S34. Infrared spectrum of *trans*-[Zn(quin)$_2$(morph)$_2$] (**12**).

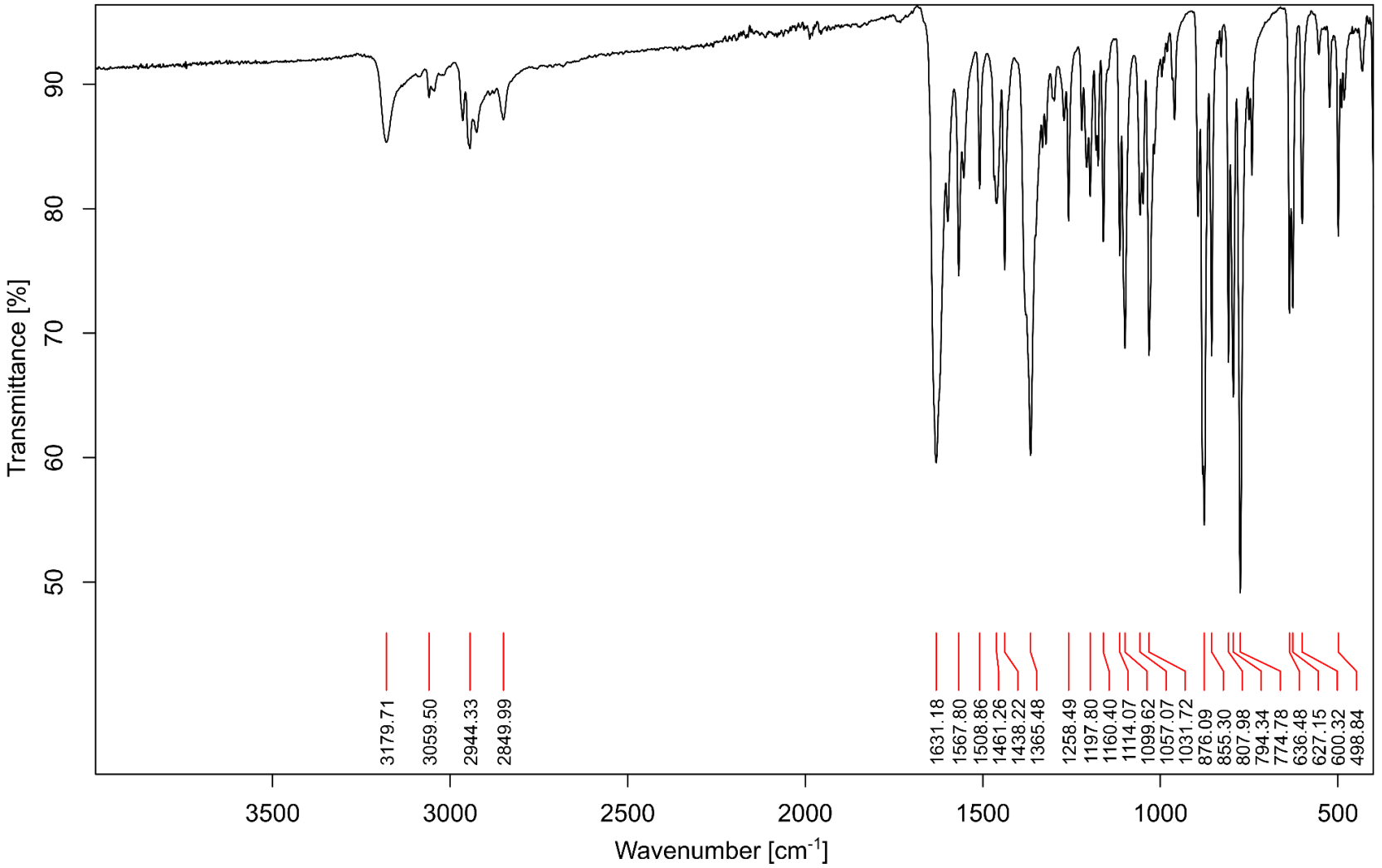

Figure S35. Infrared spectrum of morphH[Zn(quin)$_3$]·CH$_3$CN (**13**).

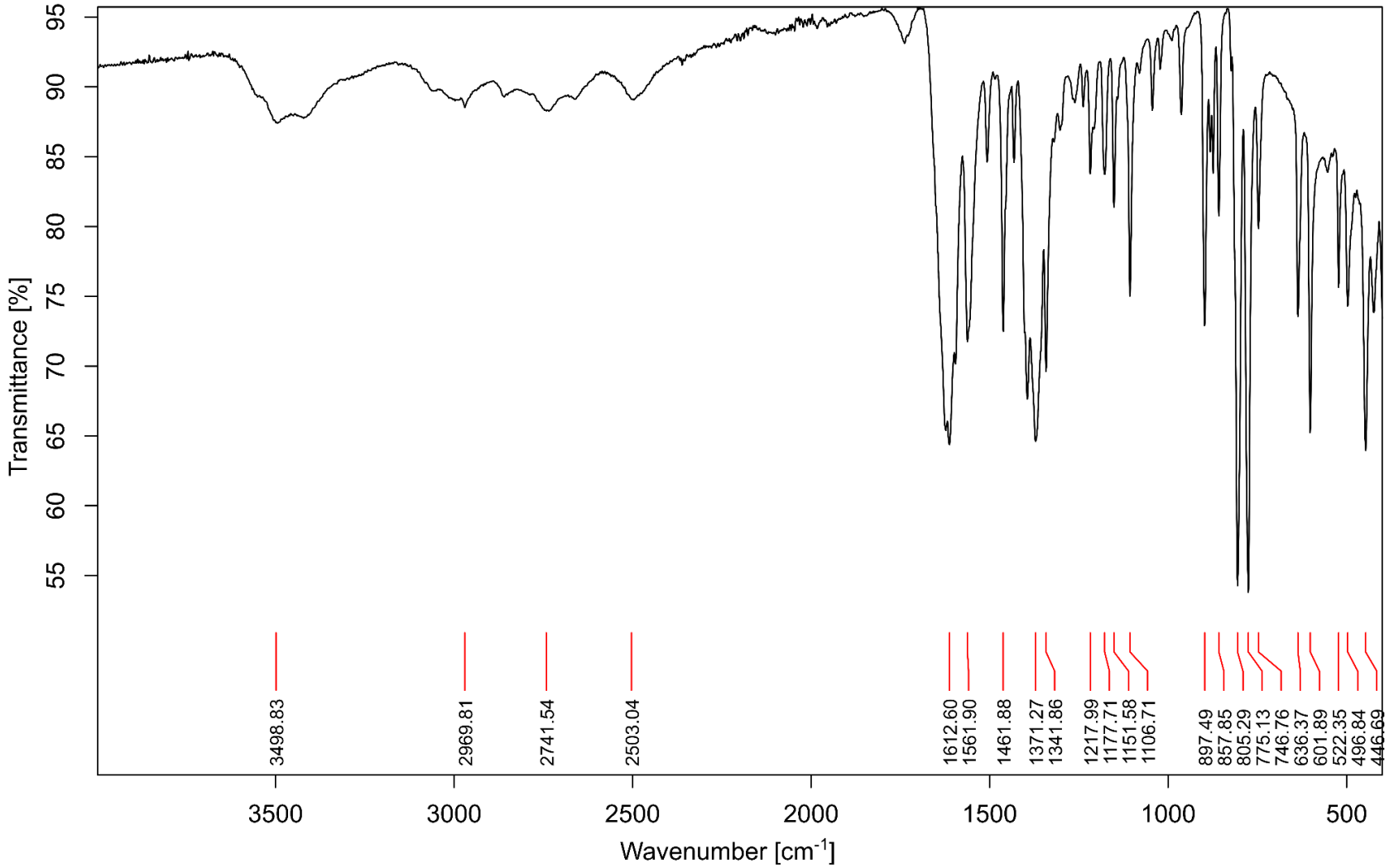

5. ^{1}H NMR spectroscopy

Table S4. Chemical shifts [ppm] in the ^{1}H NMR spectra of compounds **1** to **13**.[a]

compound	complex[b]	quinaldinate	amine
1	*trans*-[Zn(quin)$_2$(pipe)$_2$]	8.94d, 8.79d, 8.41d, 8.20d, 8.04–8.01m, 7.84–7.81m	2.62–2.60m, 1.45–1.40m, 1.38–1.34m
2	[Zn(quin)$_2$(pipe)]·*cis*-[Zn(quin)$_2$(pipe)$_2$]	8.94d, 8.80d, 8.42d, 8.21d, 8.04–8.01m, 7.84–7.81m	2.63–2.61m, 1.43–1.40m, 1.39–1.34m
7	[Zn(quin)$_2$(pyro)$_2$][c]	8.93d, 8.79d, 8.40d, 8.20d, 8.03–8.00m, 7.84–7.81m	2.64–2.62m, 1.52–1.47m
12	*trans*-[Zn(quin)$_2$(morph)$_2$]	8.86d, 8.79d, 8.41d, 8.20d, 8.03–8.00m, 7.83–7.81m	3.49–3.47m, 2.65–2.63m
		quinaldinate	**amineH$^+$**
3	[Zn(quin)$_3$]$^-$, six-coordinate	8.59d, 8.55d, 8.20d, 8.05d, 7.75–7.72m, 7.67–7.64m	2.98–2.96m, 1.62–1.57m, 1.52–1.48m
8	[Zn(quin)$_3$]$^-$, six-coordinate	8.58d, 8.55d, 8.19d, 8.05d, 7.76–7.73m, 7.68–7.65m	3.09–3.06m, 1.83–1.78m
13	[Zn(quin)$_3$]$^-$, six-coordinate	8.60–8.57m, 8.21d, 8.07d, 7.79–7.76m, 7.70–7.67m	3.71–3.69m, 3.03–3.01m
		quinaldinate	**amidine**
4a	[Zn(quin)$_2$(pipeam)]	8.78d, 8.50d, 8.35d, 8.21d, 8.00–7.97m, 7.83–7.80m	6.98s, 3.25–3.23m, 1.90s, 1.46–1.42m, 1.23m
10a	[Zn(quin)$_2$(pyroam)]	8.77d, 8.54d, 8.34d, 8.20d, 7.98m, 7.81m	3.28m, 3.10m, 1.94s, 1.76–1.73m
		quinaldinate	**amidineH$^+$**
11	[Zn(quin)$_3$]$^-$ [d]	8.58d, 8.53d, 8.18d, 8.04d, 7.74–7.71m, 7.66–7.63m	8.93s, 3.54t, 3.32t, 2.21s, 1.97–1.86m
5	[Zn(quin)$_3$]$^-$, five-coordinate	8.58d, 8.53d, 8.18d, 8.04d, 7.74–7.71m, 7.66–7.63m	9.01s, 3.51–3.49m, 2.23s, 1.62–1.55m
		quinaldinate	**amidineH$^+$** or **amineH$^+$**
6	[Zn(quin)$_2$(CH$_3$COO)]$^-$	8.72–8.71m, 8.31d, 8.16d, 7.93–7.90m, 7.79–7.76m	3.49–3.47m, 2.22s, 1.62–1.55m
9	[Zn(quin)$_2$Cl]$^-$	8.78–8.74m, 8.32d, 8.19d, 7.99–7.96m, 7.82–7.79m	8.51s, 3.10–3.06m, 1.83–1.78m

[a] Splitting patterns are denoted as s (singlet), d (doublet), t (triplet) and m (multiplet).

[b] Formula of a complex species in the solid state, as revealed by the X-ray structure analysis.

[c] The composition could not be verified by the X-ray structure analysis.

[d] Undefined mixture of **11triclinic** and **11monoclinic** was used for analysis. The sample contained both forms of the [Zn(quin)$_3$]$^-$ ions.

Figure S36. ^{1}H NMR spectrum of [Zn(quin)$_2$(pipe)$_2$]·2CH$_3$CN (**1**) in DMSO-d_6.

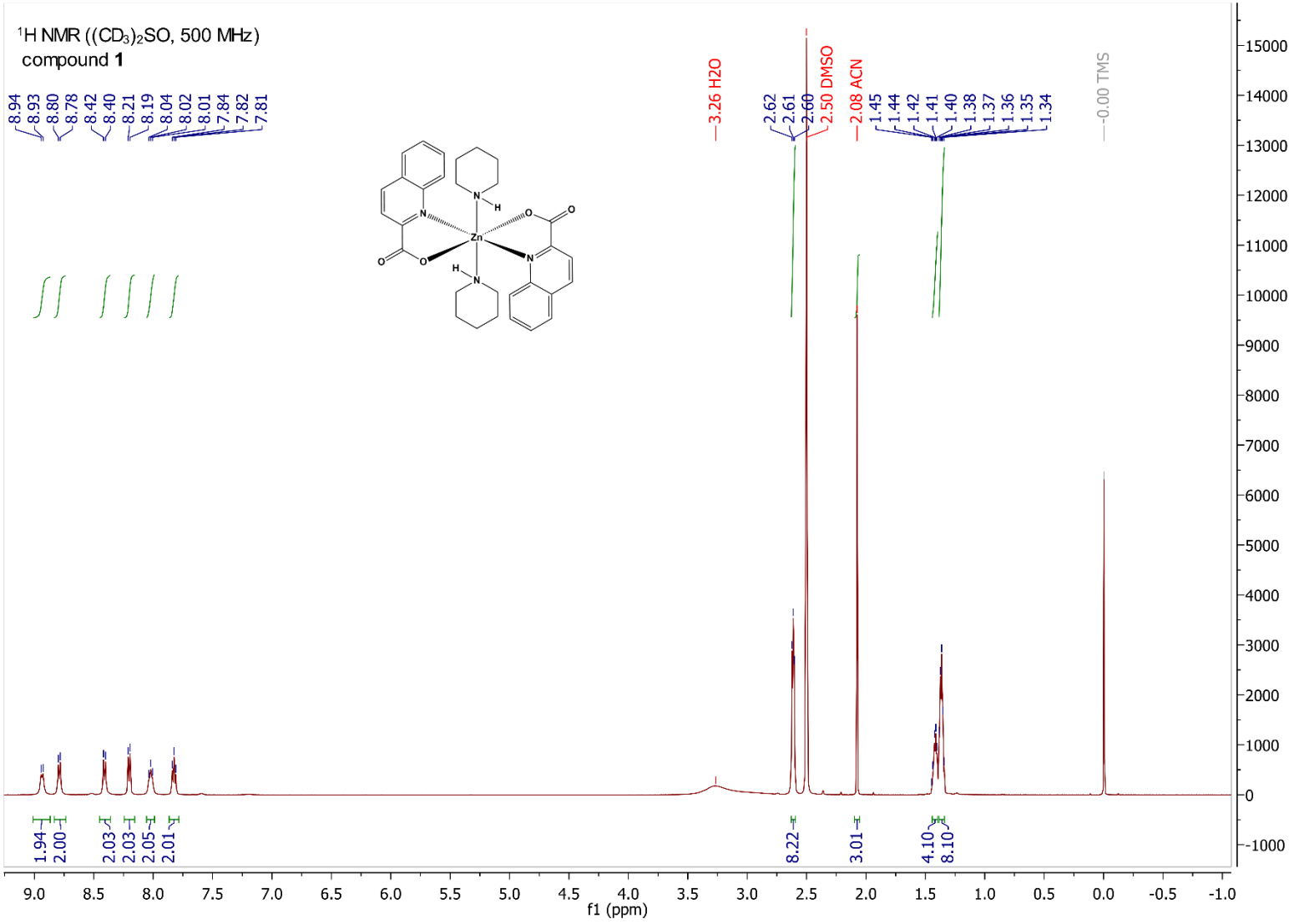

Figure S37. ^{1}H NMR spectrum of [Zn(quin)$_2$(pipe)]·*cis*-[Zn(quin)$_2$(pipe)$_2$] (**2**) in DMSO-d_6.

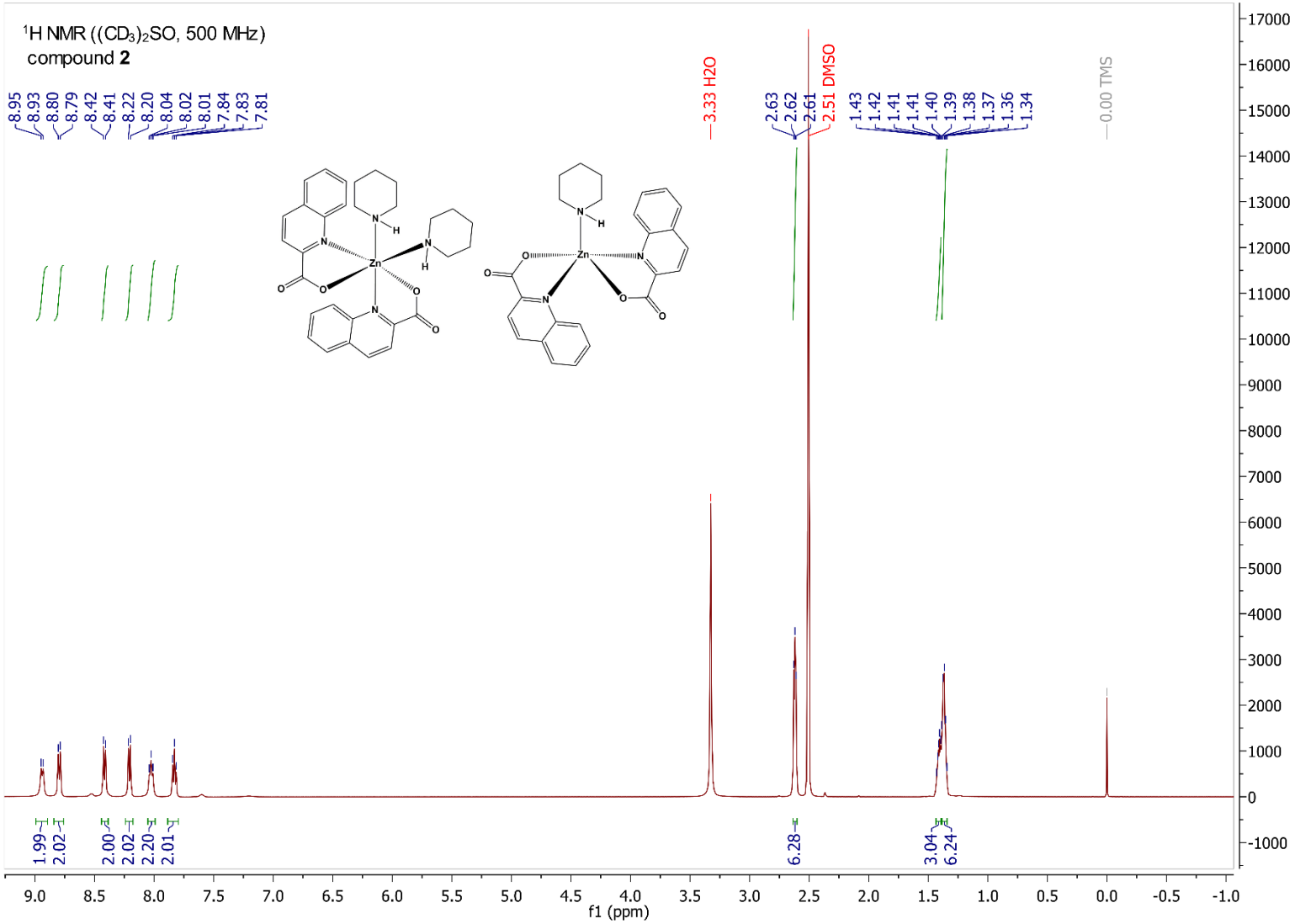

Figure S38. ^{1}H NMR spectrum of pipeH[Zn(quin)$_3$]·CH$_3$CN (**3**) in DMSO-d_6.

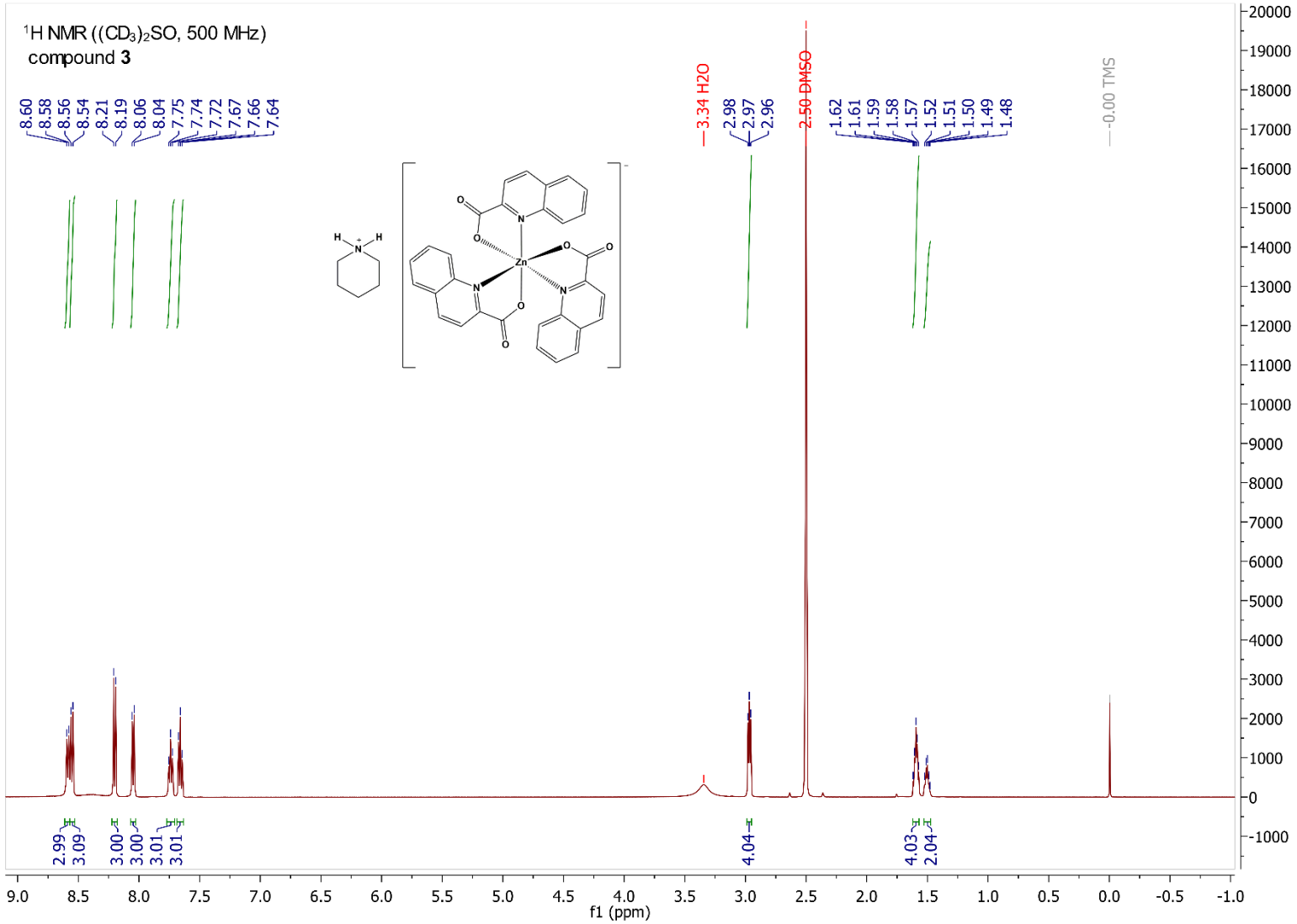

Figure S39. ^{1}H NMR spectrum of [Zn(quin)$_2$(pipeam)]·CH$_3$CN (**4a**) in DMSO-d_6.

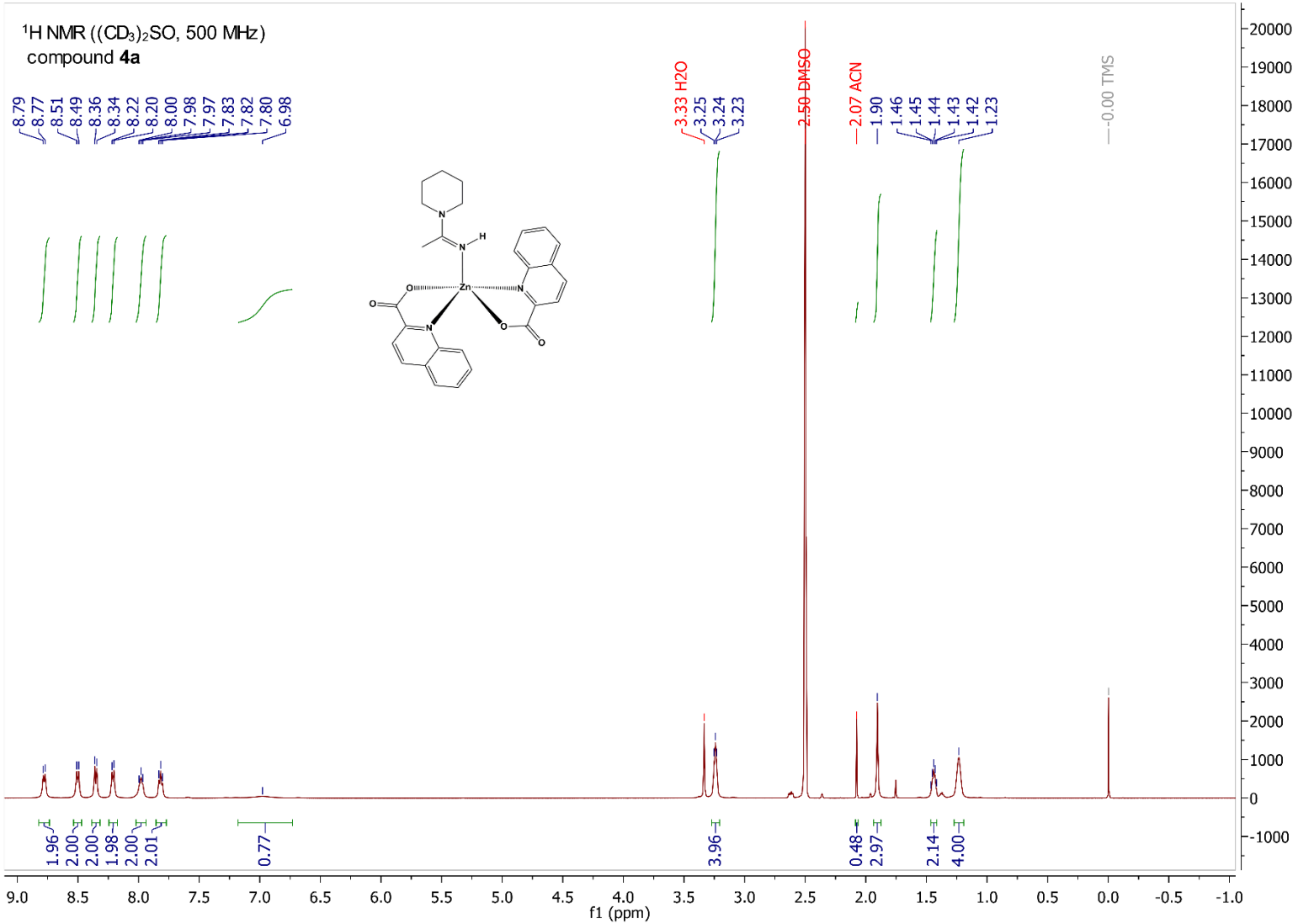

Figure S40. ^{1}H NMR spectrum of pipeamH[Zn(quin)$_3$] (**5**) in DMSO-d_6.

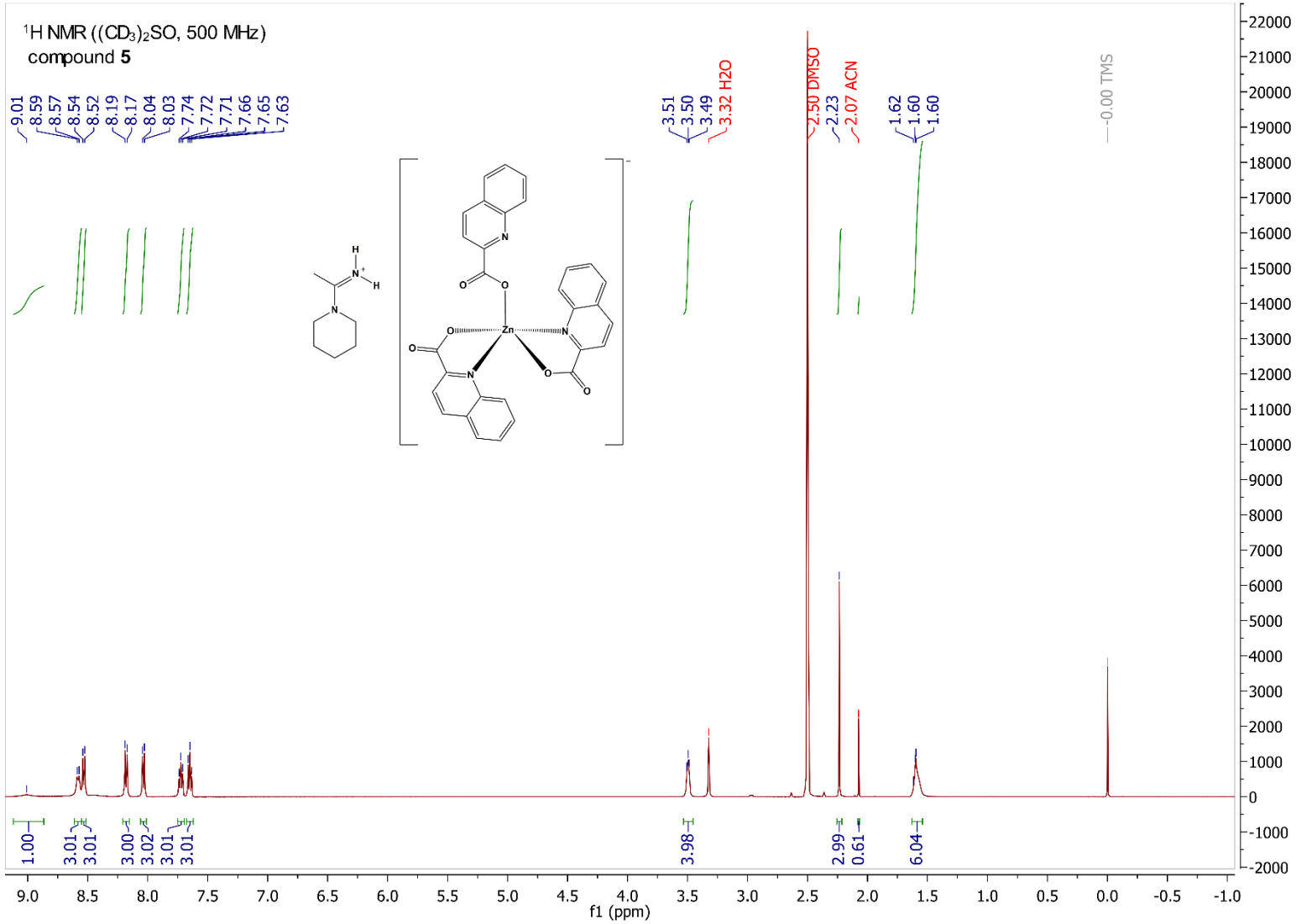

Figure S41. ^{1}H NMR spectrum of pipeamH[Zn(quin)$_2$(CH$_3$COO)]·acetamide (**6**) in DMSO-d_6.

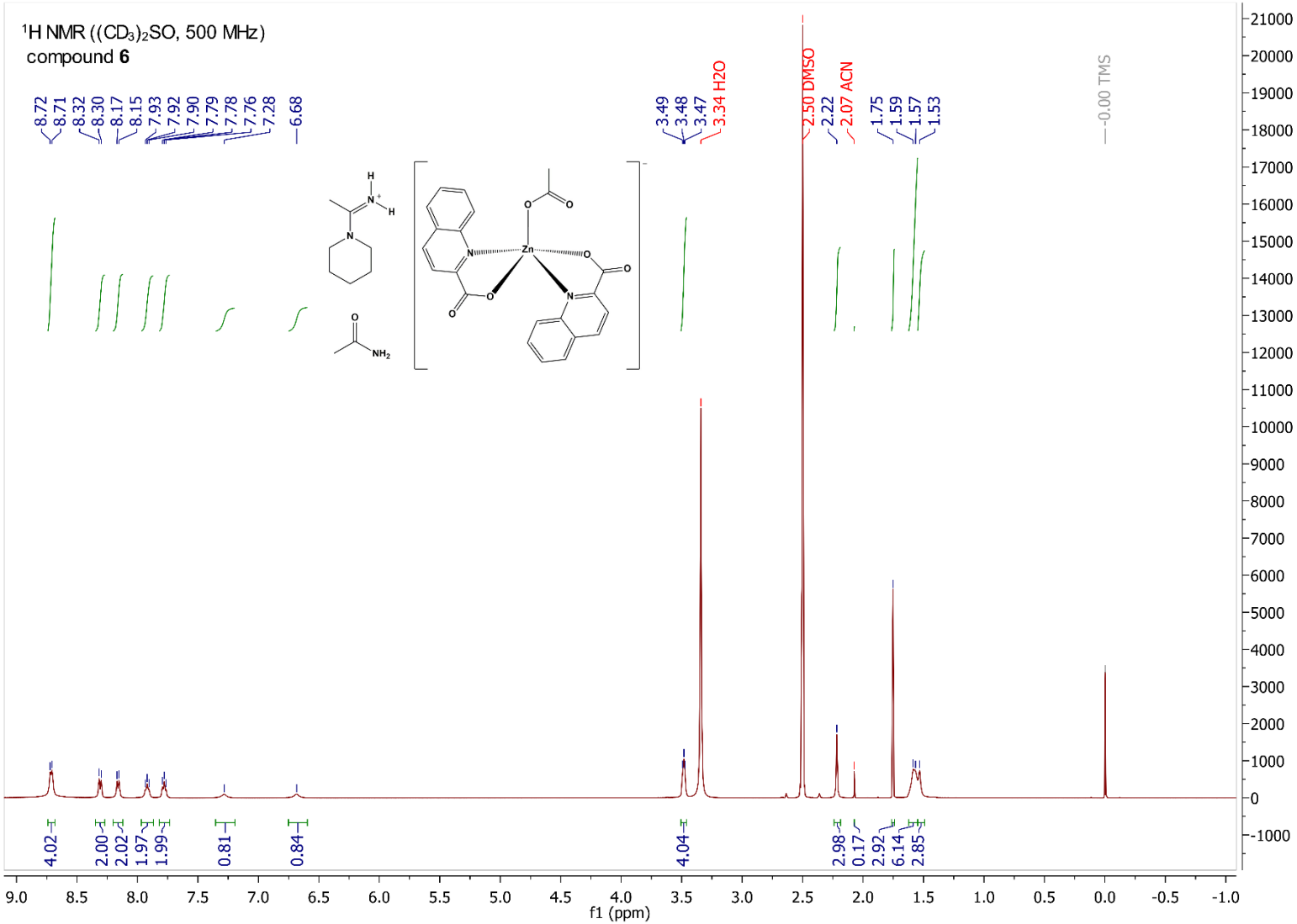

Figure S42. ^{1}H NMR spectrum of [Zn(quin)$_2$(pyro)$_2$] (**7**) in DMSO-*d*$_6$.

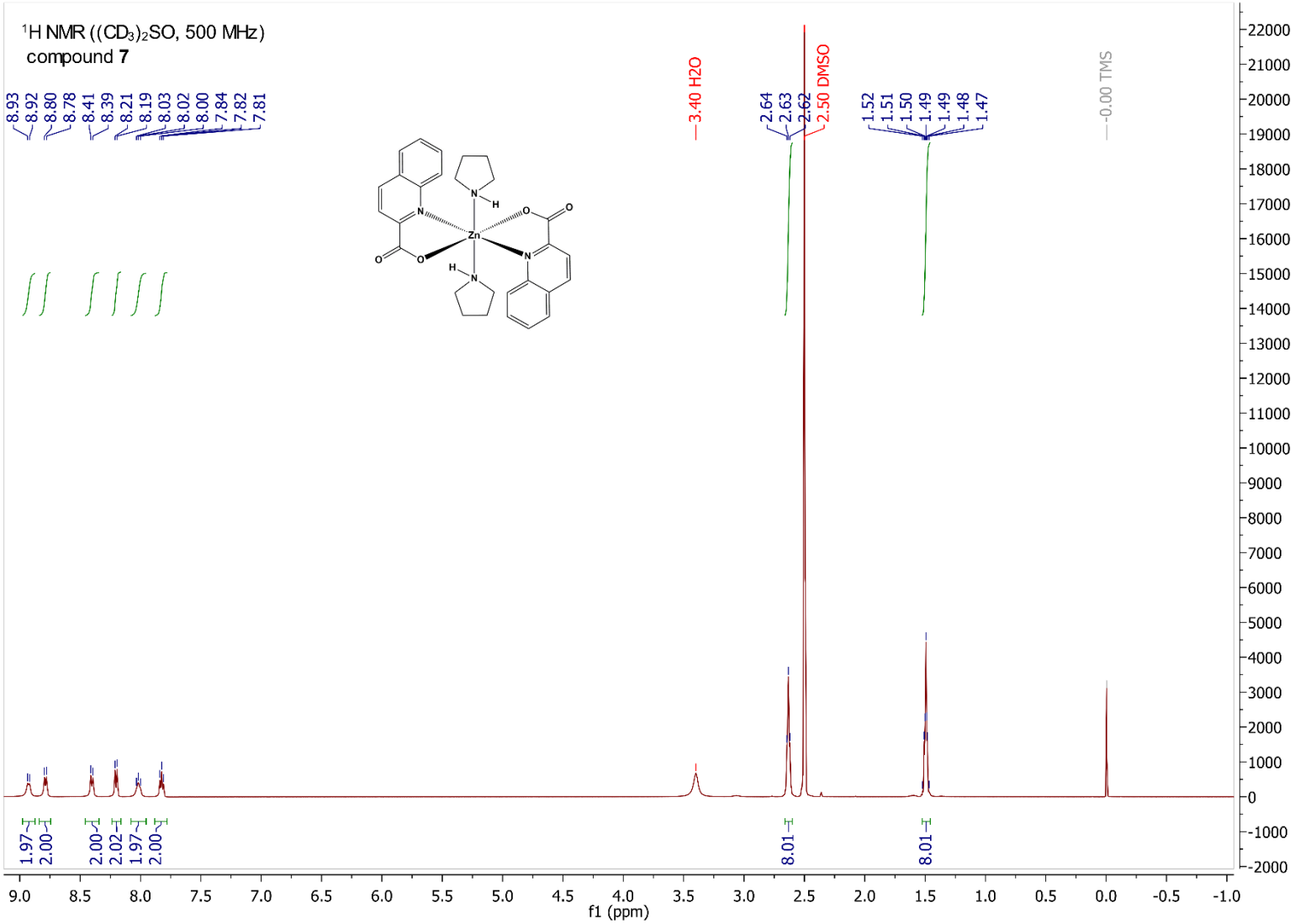

Figure S43. ^{1}H NMR spectrum of pyroH[Zn(quin)$_3$]·CH$_3$CN (**8**) in DMSO-d_6.

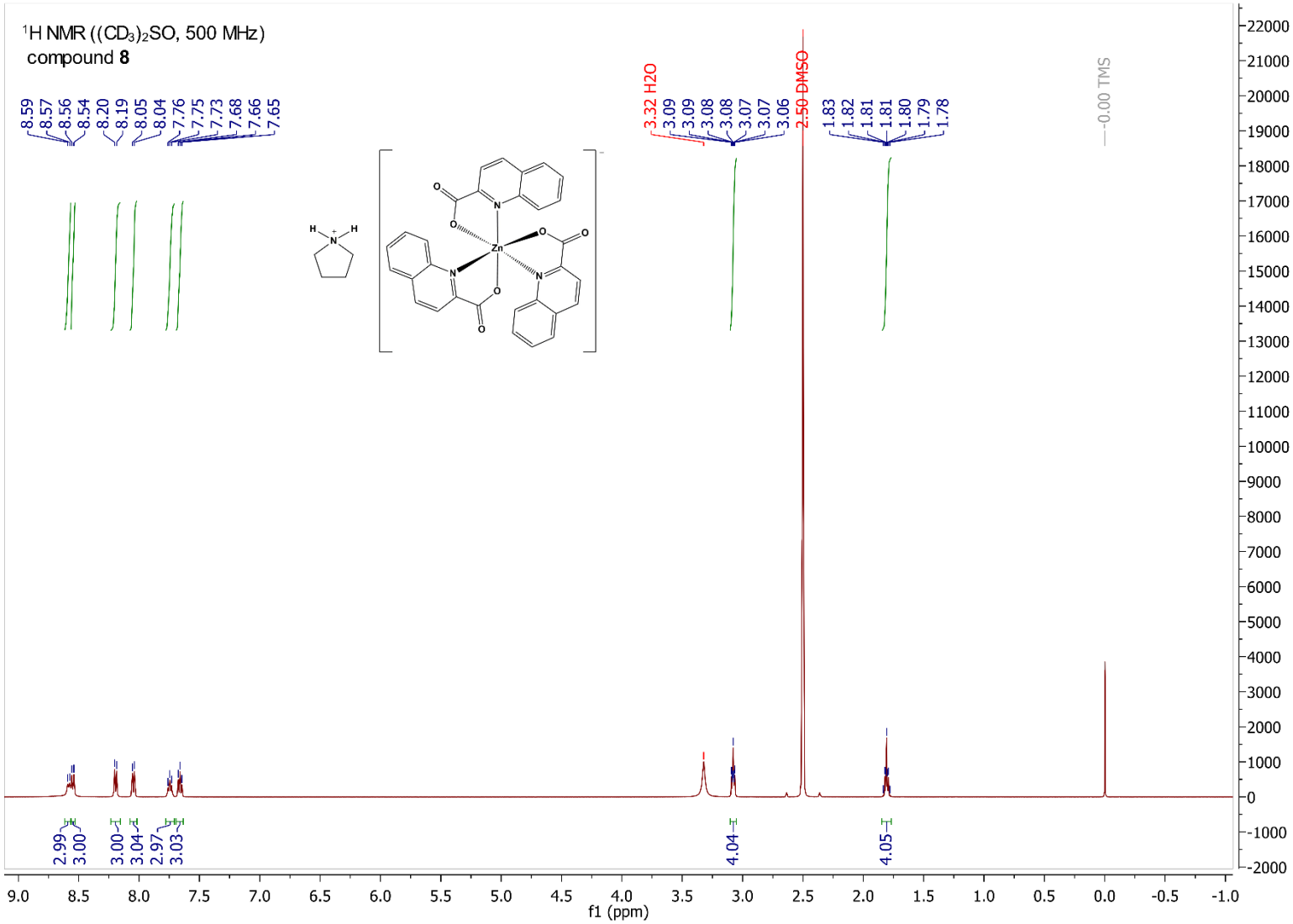

Figure S44. ^{1}H NMR spectrum of pyroH[Zn(quin)$_2$Cl] (**9**) in DMSO-d_6.

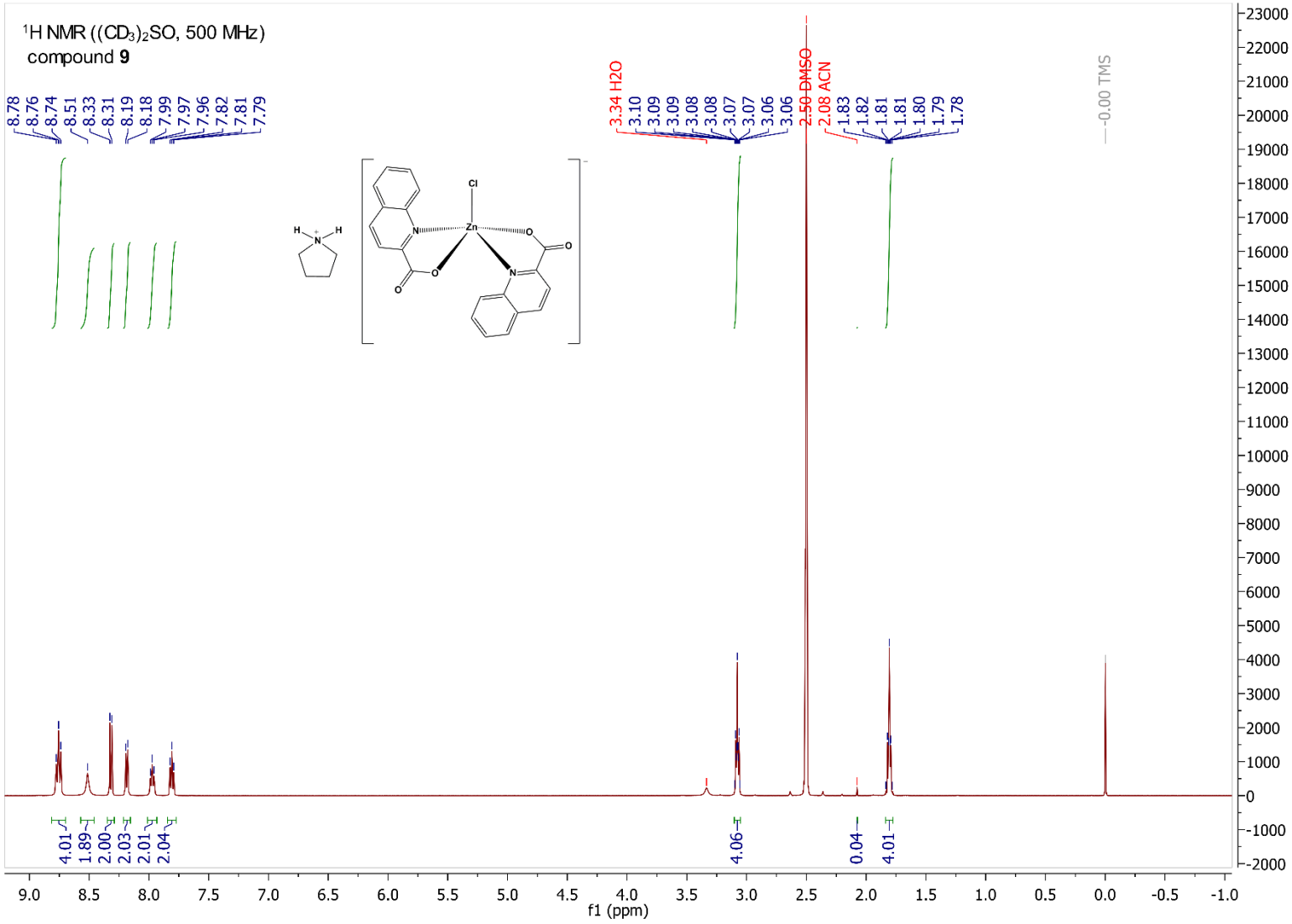

Figure S45. ^{1}H NMR spectrum of [Zn(quin)$_2$(pyroam)]·CH$_3$CN·0.5pyroAm·0.5H$_2$O (**10a**) in DMSO-d_6.

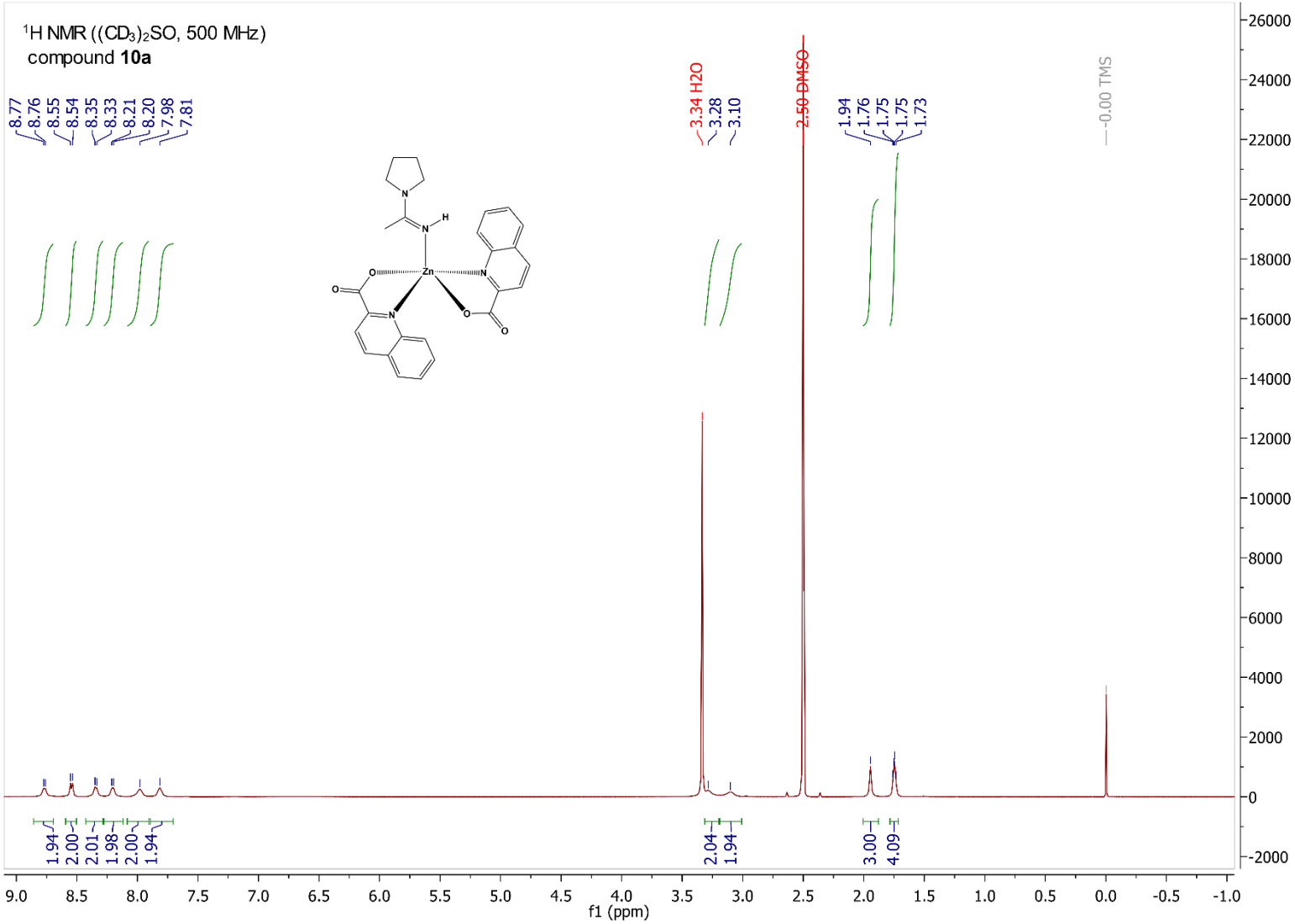

Figure S46. ^{1}H NMR spectrum of pyroamH[Zn(quin)$_3$] (**11**) in DMSO-d_6.

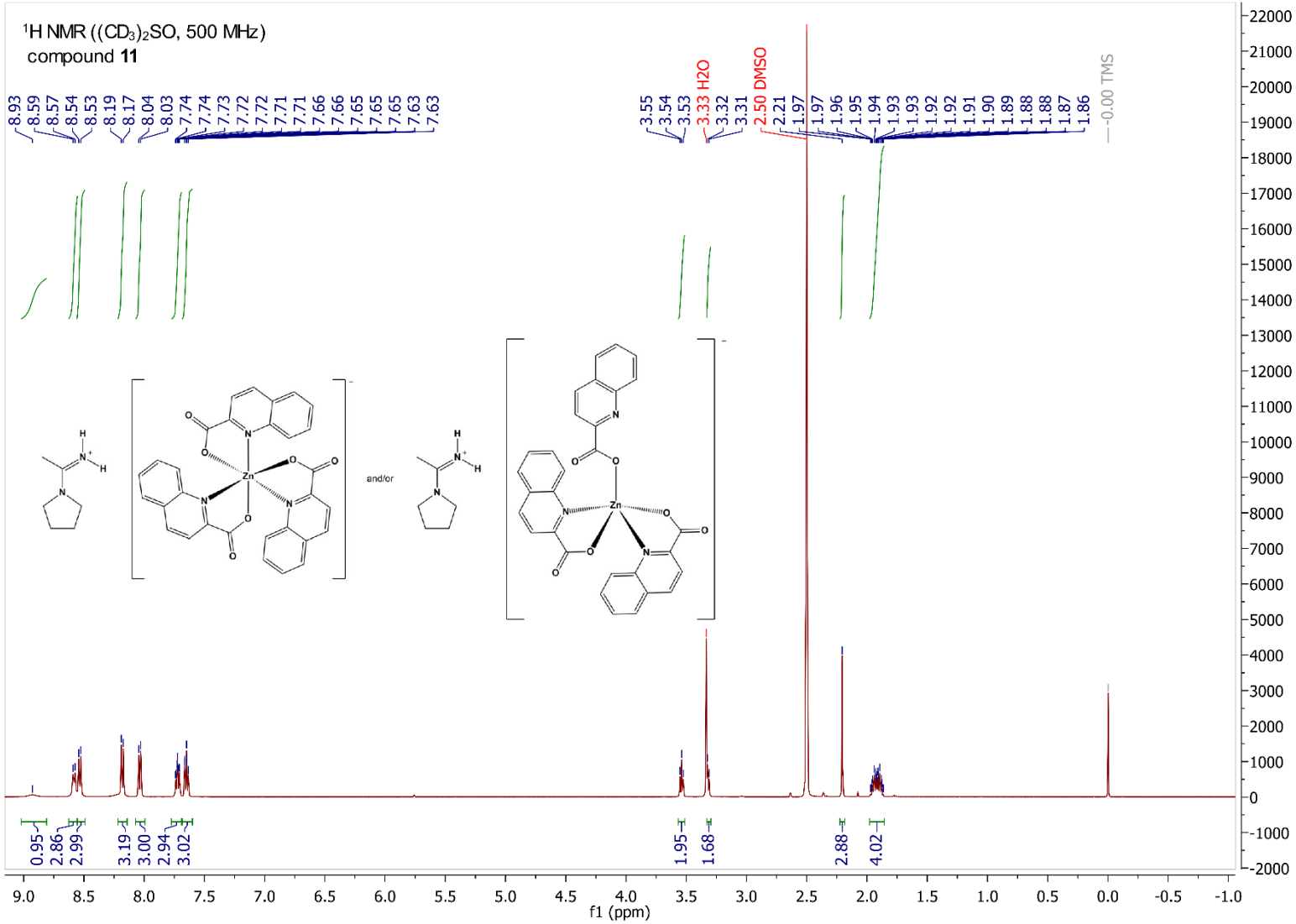

Figure S47. ^{1}H NMR spectrum of *trans*-[Zn(quin)$_2$(morph)$_2$] (**12**) in DMSO-d_6.

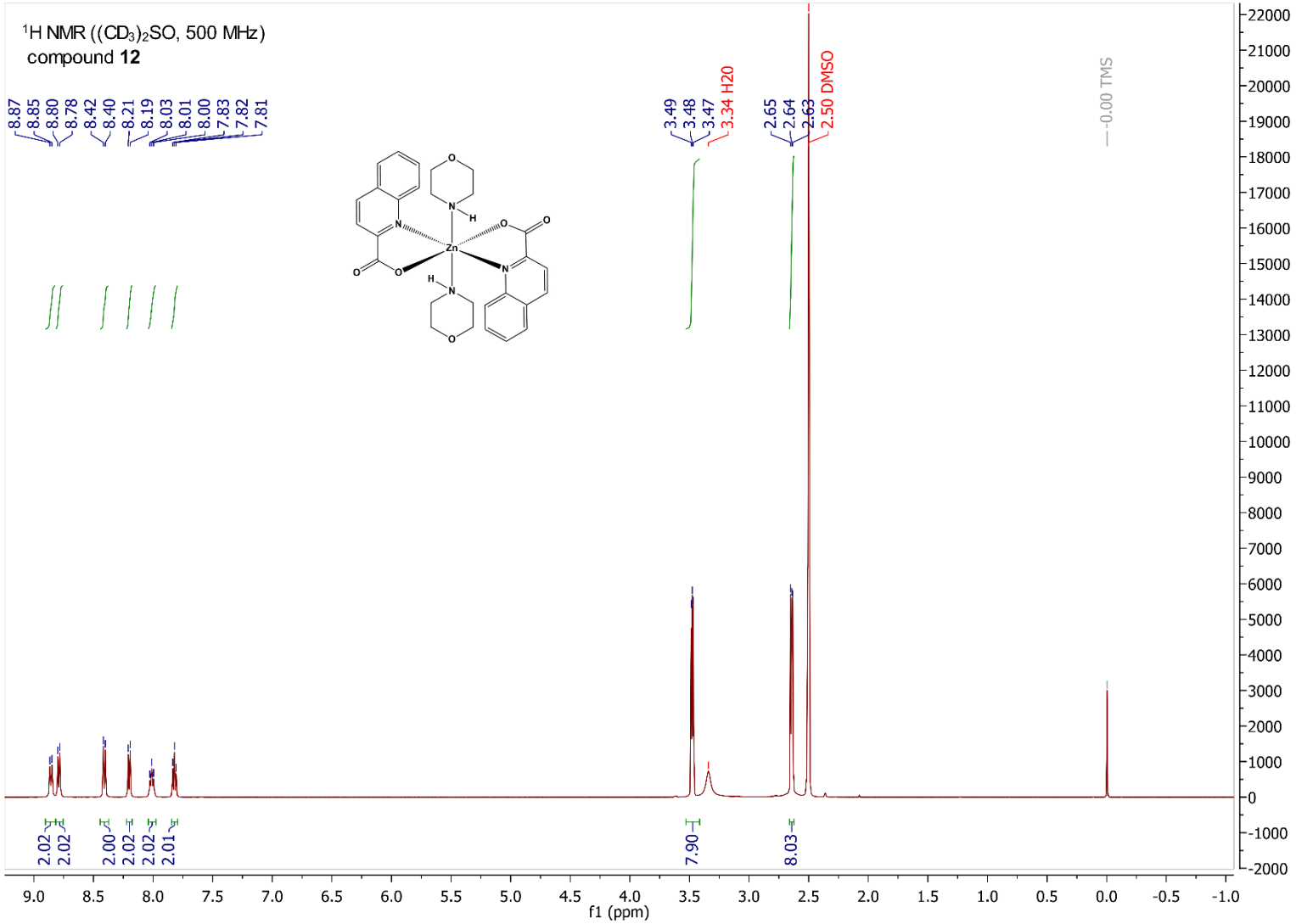

Figure S48. ^{1}H NMR spectrum of morphH[Zn(quin)$_3$]·CH$_3$CN (**13**) in DMSO-d_6.

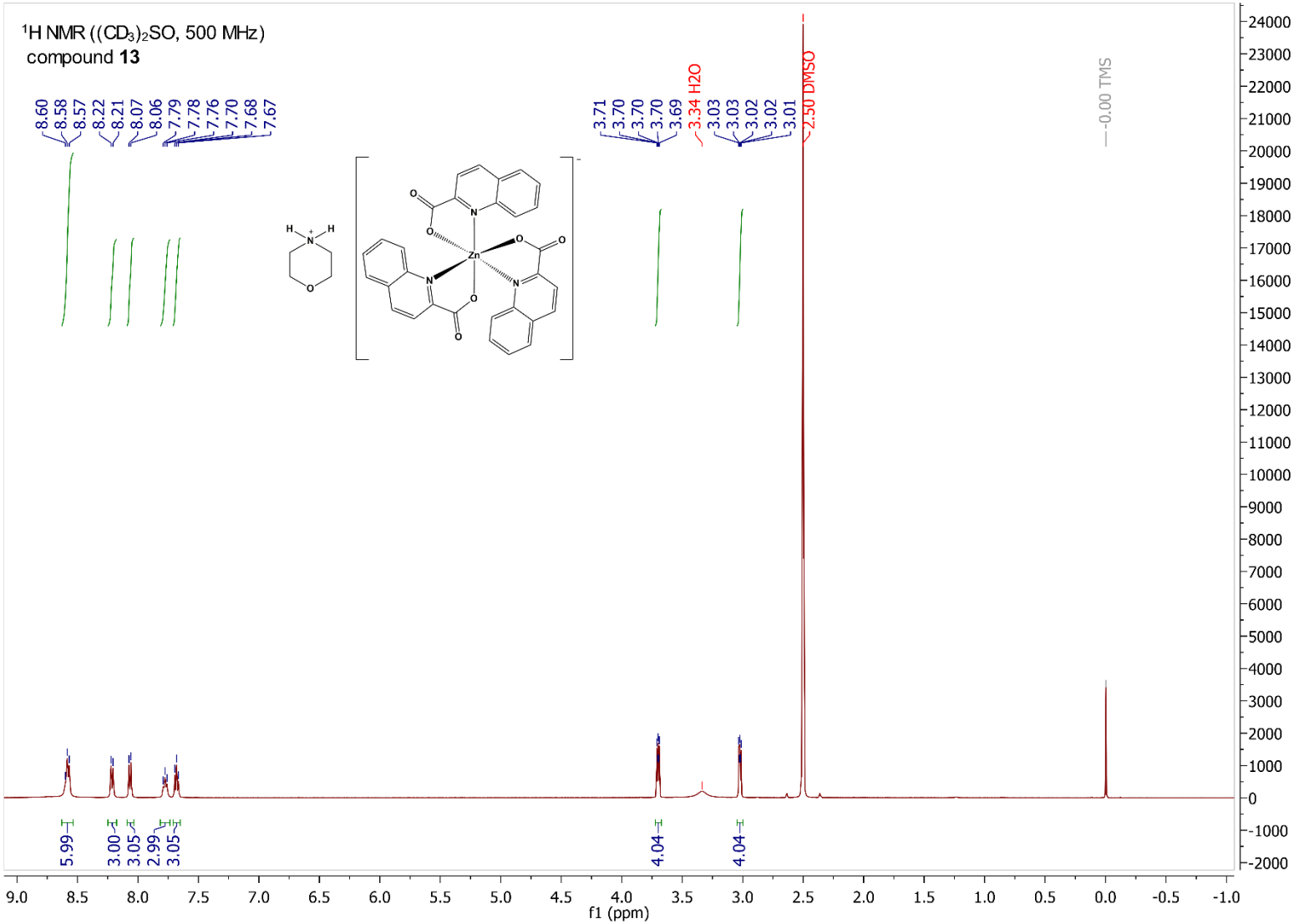

6. References

S1. C. F. Macrae, I. J. Bruno, J. A. Chisholm, P. R. Edgington, P. McCabe, E. Pidcock, L. Rodriguez-Monge, R. Taylor, J. van de Streek and P. A. Wood, *J. Appl. Crystallogr.*, 2008, **41**, 466-470.

S2. M. C. Etter, J. C. MacDonald and J. Bernstein, *Acta Crystallogr., Sect. B*, 1990, **46**, 256-262.

S3. A. L. Spek, *Acta Crystallogr., Sect. D*, 2009, **65**, 148-155.